# Advanced Numerical Simulation of Composite Woven Fabric Forming Processes

Abel Cherouat, Houman Borouchaki

# Advanced numerical simulation of composite woven fabric forming processes

**A. Cherouat*** **and H. Bourouchaki**

University of Technology of Troyes, Charles Delaunay Institute/GAMMA3-INRIA Project Team, Troyes, France

Different approaches used for the simulation of woven reinforcement forming are investigated. Especially several methods based on geometrical and finite element approximations are presented. Some are based on continuous modelling, while others called discrete or mesoscopic approaches, model the components of the dry or prepregs woven fabric. Continuum semi discrete finite element made of woven unit cells under biaxial tension and in-plane shear is detailed. In continuous approaches, the difficulty lies in the necessity to take the strong specificity of the fibre directions into account. The fibres directions must be strictly followed during the large strains of the fabric. In the case of geometrical or continuum approaches (semi-discrete) the directions of the fibres are naturally followed because the fibres are modeled. Explicitly, however, modeling each component at the mesoscopic scale can lead to high numerical cost. During mechanical simulation of composite woven fabric forming, where large displacement and relative rotation of fibres are possible, severe mesh distortions occur after a few incremental loads. Hence an automatic mesh generation with remeshing capabilities is essential to carry out the finite element analysis. Some numerical simulations of forming process are proposed and compared with the experimental results in order to demonstrate the efficiency of the proposed approaches.

**Keywords:** Composite woven fabric, finite element analysis, geometrical approach, composite forming, remeshing procedure

* University of Technology of Troyes, Charles Delaunay Institute/GAMMA3-INRIA Project Team, 12 rue Marie-Curie, BP 2060, 10010 Troyes, France, Email: abel.cherouat@utt.fr, Tel +33 3 25 71 56 74 & Fax. +33 3 25 51 59 11 20

# 1. INTRODUCTION

Polymer composite reinforced by woven fabric (glass, carbon or kevlar) is known to have high specific stiffness and, in combination with automatic manufacturing processes, make it possible to fabricate complex structures (aircraft, boat, automotive, etc) with high level of weight and cost efficiency. As known, the substitution of metal alloys by composite materials, in general, reduces structural mass by 20-30%. The mass increase is due also to the numerous variety of semi-products (roving, fabrics, knitted fabrics, braids pre-impregnated or not) permitting the development of new structures. Fabrication processes, also, have undergone substantial evolution in recent years. Although the traditional lay-up process will remain the process of choice for some applications, new developments in Resin Transfer Molding (RTM) or Sheet Molding Compound (SMC), low temperature curing prepregs and low pressure molding compounds have matured significant are reached, and are now being exploited in high technology areas such as aerospace industry. For example, by using such composites, the automotive industry can realize improved fuel economy through vehicle-weight reduction by replacing the currently used steel and aluminium parts with thermoplastic composites with the added benefit of a corrosion-resistant material. The choice of manufacturing process depends on the type of matrix and fabric, the temperature required to form the part and the cost effectiveness of the process. In particular, thermo-forming is a promising manufacturing process for producing high-volume low-cost composite parts using commingled fibreglass/polypropylene woven fabrics [1-3].

The simulation of the manufacturing of a textile reinforced composite part with a Liquid Composite Moulding-like process, which involves draping (or deep-drawing) and impregnation of the preform, includes several stages (see Figure 1). First, a mould is designed with CAD software, and the CAD model is meshed. Then, a draping (or deep-drawing) simulation tool is used to compute the deformations of the textile layers inside the mould. As a result, for every element of the mesh, textile parameters like the shear angle and the thickness of the layer are available. With these parameters given, the local (meso-scale) properties for every element is determined (pre-processing), and given as input for the macroscopic structure after resin polymerization simulation. The result of the macro-simulation is then post-processed to optimize the mechanical properties of composite structure. The numerical simulation of composite forming is an efficient means of evaluating factors related to manufacturing processes and an efficient help to design pre-forming sequence for the manufacturing of fabric reinforced composites. It is possible to detect main problem occurring during the shaping deformation and to obtain good quantitative information on the forming process [2-8].

Different levels of modeling intervene in the simulation of woven reinforcement forming (1) architecture design level, (2) preliminary design level, (3) mechanical level by computational software and (4) optimisation level [6-8]. Most of these levels are integrated and take into account specific constraints of manufacturing processes. The particular form of composite fabrication (Pre-preg) begins with the pre-impregnation of reinforcement materials with a resin. The combining of these two materials occurs prior to the moulding process and therefore enables a very accurate reinforcement to resin ratio to be achieved. Pre-preg materials are used extensively in the aerospace or automotive industry due to their ability to maximize strength to weight ratios. Pre-pregs are pliable and therefore able to be cut into

various shapes or patterns prior to processing into the moulded products. But for the manufacturing of non-developable composite part (part that can not make flat un-stretched), a new problem intervenes in the design chain resulting from the number of parameters influencing the global behavior of composite forming process. The ability to define, in advance, the ply shapes and material orientation allowed the engineers to optimize the composite structural properties of the composite products for maximum strength, maximum material utilization and maximum lay-up efficiency [10-20].

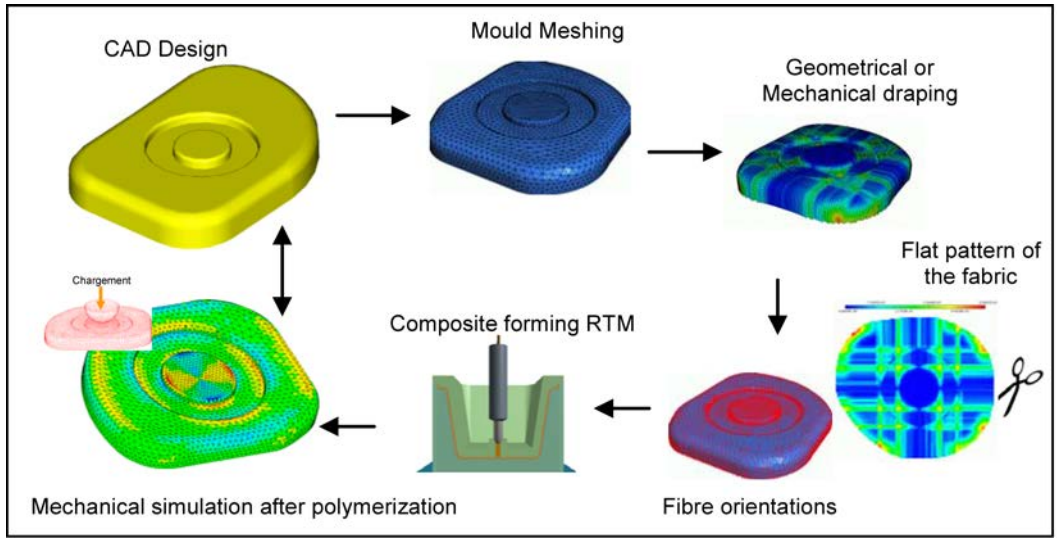


Figure 1. Illustration of the manufacturing of a textile reinforced composite part.

The composite manufacturing process involves large displacements and rotations and large shear of weft and warp fibres, which can have a significant effect on the processing and structural properties of the finished product. The formulation of new and more efficient numerical models for the simulation of the shaping composite processes must allow for reduction in the delay in manufacturing of complex parts and an optimization of costs in an integrated design approach [3, 20-25]. Several modelling approaches have been developed to account for the evolution of the orthotropic directions during high shearing, and these approaches include the geometrical and the finite element approaches. The geometrical approach so called fishnet algorithms is used to determine the deformed shape of draped fabrics. This method, where the fabric is placed progressively from an initial line, provides a close enough resemblance to handmade draping [26-30]. They are very fast and fairly efficient in many prepreg draping cases. Nevertheless, this method has major drawbacks. They account neither for the mechanical behaviour of the fabric nor for the static boundary conditions. This last point is very important in the case of forming with punch and die (such as in the pre-forming of the RTM process). The loads on the tools, especially on the blank-holder, influence the quality of the shaping operation, and therefore, need to be considered in simulations and therefore, need to be considered in simulations [31-34].

The alternative to the geometrical approach consists of a mechanical analysis of the fabric deformation under the boundary conditions prescribed by the forming process. This requires a specific model of the woven reinforcement and its mechanical behaviour. The

mechanical behaviour of woven fabrics is complex due to the intricate interactions of the fibres. It is a multi-scale problem. The macroscopic behaviour is very much dependent on the interactions of fibres at the mesoscale (scale of the woven unit cell) and at the micro-scale (level of the fibres constituting yarns). Despite of a great amount of work in the field, there is no widely accepted model that accurately describes all the main aspects of fabric mechanical behaviour. The main model families come from the multi-scale nature of the textile. A first family of models is obtained by homogenizing the mechanical behaviour of the underlying meso-structure and considering the fabric as an anisotropic continuum [9, 12, 15-20]. If these models can easily be integrated in standard finite element using conventional shell or membrane elements, then the identification of homogenized material parameters is difficult, especially because these parameters change when the fabric is strained and when, consequently, the directions and the geometry (crimp, transverse sections…) of the fibres change. Some of these approaches will be described, especially a non-orthogonal constitutive model [35-40] and an anisotropic hypoelastic continuous behaviour for fibrous material based on an objective derivative using the rotation of the fibre [34-35]. Conversely, some authors present fully discrete models of fabrics [41-44]. Each yarn or each fibre is modelled and is assumed to be a straight or a curved beam or truss. Sometimes they are modeled as 3D domains [42]. Springs are often used to model warp and weft yarn interactions. In the objective of fabric forming simulations, some authors extend the discrete modelling to the whole textile structure that is represented by a network of interwoven trusses or beams with different tensional and rotational springs. Accounting for the simplicity of each component, the whole textile structure deformation can be computed.

Nevertheless, the computational effort needed is relatively significant. At present this method is restricted to simple geometry of the local yarn and relatively simple mechanical behaviour. When a fine model of the fibrous yarns is used, the analysis can only consider a small part of the textile reinforcement such as a few woven or knitted cells. The semi-discrete approach is a compromise between the above continuous and discrete approaches [20, 25, 36-39]. A finite element method is associated to a mesoscopic analysis of the woven unit cell. Specific finite elements are defined that are made of a discrete number of woven unit cells. The mechanical behaviour of these woven cells is obtained by experimental analyses or from 3D FE computations of the woven cell. The nodal interior loads are deduced from this local behaviour and the corresponding strain energy in the element deformation.

In current study, the geometrical and the finite element semi-discrete approaches are used to simulate the deformation of composite fabrics by shaping process. These approaches, while giving good results and being efficient in terms of computing time, are generally somewhat complex and sometimes very challenging to implement into commercially available FEA packages.

The geometrical approach is well adapted to preliminary design level. It is based on geometrical aspects of the warping. Our method is based on a modified "MOSAIC" algorithm, which is suitable to generate a regular quad mesh representing the lay-up of the curved surfaces (giving the exact fibre orientations). The method is implemented in the GeomDrap software [45] which is now integrated in the ESI-Pam software [23]. This software provides a fibre quality chart (showing the fibre distortions, the rate of falling and the rate of draped surface) to predict local folding due to overlapping of fibers in the shear exceeds limit value (up to 60° in some cases). It can be used to optimize the draping process (with respect to the above quality measure) by improving the lay-up directions or the marker

data location. The lay-up of complex curved surfaces can be made in a few seconds [17, 27-33].

The mechanical approach is base on a meso-structural description for finite deformations and geometrical non-linearity. The not polymerized resin has a viscous behavior and the reinforced fibers are treated as either unidirectional non linear elastic behavior. The unit cell of the mesoscopic model used here for a plain-weave fabric consists of bi-component finite elements. The tensile load is carried by the 1-D elements that will capture the changes in the orthotropic directions during the shearing. The 2-D element accounts only for the shearing resistance of the fabric and hence has no tensile stiffness. The bi-component finite elements for modeling composite fabric behavior are based on 3D membrane finite elements representative of resin behavior and truss finite elements representative of warp and weft fibers behavior. The efficiency of the proposed model resides in the simplicity of its finite element discretization and the performance of its mechanical background [46-47-50].

Due to large displacement due to forming process, the bi-component finite element mesh representing the workpiece undergoes severe shear of fibres hence, necessitates remeshing or the generation of a new mesh for the deformed/evolved geometric representation of the computational domain [51-55]. It is therefore necessary to update the mesh in such a way that it conforms to the new deformed geometry and becomes dense enough in the critical region while remaining reasonably coarse in the rest of the domain. In this paper we give the necessary steps to remeshing a mechanical composite structure subjected to large displacement. An important part is constituted by geometric and physical error estimates. A three dimensional finite element analysis has been performed using the explicit finite element formulation.

## 2. GEOMETRICAL APPROACH OF COMPOSITE FABRIC FORMING

The draping of composite fabric using a mechanical approach requires the resolution of equilibrium PDE's problems by the finite element method (see section 3). In general, in the case of complex surfaces, the boundary conditions are not well defined and the contact between the surface and the fabric is difficult to manage. Furthermore, the resolution of such a problem can be too long in CPU time and is detrimental to the optimization stage of draping regarding the initial fibre directions. All of these facts lead us to consider rather a geometrical approach which is very fast and more robust allowing simultaneously to define the stratification sequences and the flat pattern for different plies and to predict difficult impregnated areas which involve manual operation like dart insertion or, on the contrary, the shortage of fabric. Based on technical criteria (mould surface covering, fabric drape covering and fibre angular distortion), this approach can constitute the pre-dimensionning or the pre-optimization stage for the manufacturing of complex composite parts. The geometrical approach is based, in general, on the fishnet method for which a fabric mesh element is subjected only to shear deformations. The difficulty of such a method is the mapping of the fabric mesh element onto any surface. Within this context, several algorithms (see [26-27, 30, 32, 55] for a synthesis), approximating the geometry of a fabric mesh element plotted onto the surface, are proposed. In particular, the edges of the fabric mesh element are approximated by line segments representing a pure estimate in the highly curved area.

In this study, we propose a new geometrical draping simulation algorithm which takes into account the true geometry of the fabric mesh element plotted onto the surface. Such a fabric mesh element is then defined by a curved quadrilateral whose edges are geodesic lines with the same length plotted onto the surface to drape. Given three vertices of the fabric mesh element on the surface, we propose an optimization algorithm to define the fourth vertex of the fabric mesh element. This algorithm allows us to drape the surface using an advancing front approach from the data of an initial start point between the fabric and the surface and the initial fibre directions at this point. In this section, continuous and discrete formulations of geometrical forming are presented. For the second formulation, we propose an algorithm of composite fabric draping without any approximation on the geometry of surface to be draped.

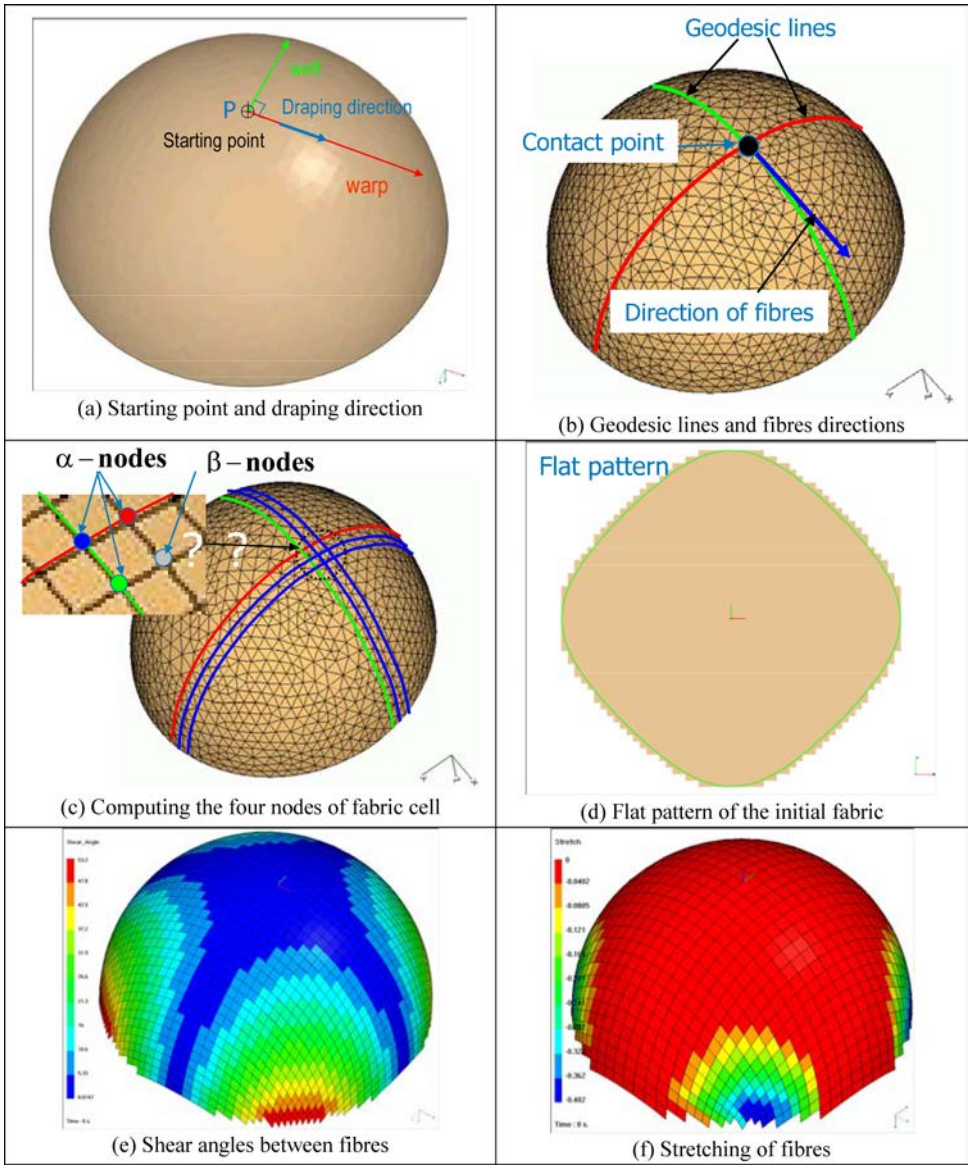


Figure 2. Geometrical draping steps.

## 2.1. Discrete Formulation

First, we present the mathematical formulation of the geometrical draping and then we propose an algorithm scheme to solve the draping problem. Let denote by $\Sigma$ the surface of the part to drape and we assume that a geometrical mesh $\mathbf{T}_{\boldsymbol{\Sigma}}$ of surface is known. Let $\mathcal{F}$ be the woven composite fabric modeled by two families (warp and weft) of mutually orthogonal and inextensible fibre described by the local coordinates $\mathrm{x} = (\xi, \eta)$. These families constitute regular quadrilateral fabric mesh $\mathbf{T}_{\mathbf{F}}$ of the fabric $\mathcal{F}$ (Figure 2 gives example of draping steps of complex part). The problem of geometrical draping of $\mathcal{F}$ onto the surface $\Sigma$ consists of calculating each node displacement of fabric mesh $\mathbf{T}_{\mathbf{F}}$ with a point of the surface mesh $\mathbf{T}_{\boldsymbol{\Sigma}}$ such that the lengths of the edge of the corresponding mesh $\mathbf{T}_{\mathbf{F}}^{\boldsymbol{\Sigma}}$ on the surface are preserved (no extensible). This problem presents infinity of solutions depending on:

1. Starting point associated with a node of fabric $\mathbf{T}_{\mathbf{F}}^{\boldsymbol{\Sigma}}$.
2. Initial warp and weft orientation $\alpha$.

Thus, to ensure a unique solution, we suppose that the points of impact on the part surface as well as the fabric orientation are given. The draping scheme is given by the following step [55]:

1. associate a starting point (corresponding to the point of impact of the machine to drape) on the surface on geometrical part mesh $\mathbf{x}_0^{\Sigma} = (\xi_0, \eta_0)$
2. compute step by step the warp nodes of $\mathbf{T}_{\mathbf{F}}^{\boldsymbol{\Sigma}}$, classified as $\alpha - \mathbf{nodes}$, from the starting point, associated with nodes $(\xi, \eta_0)$ of $\mathbf{T}_{\mathbf{F}}$,
3. compute step by step the weft nodes of $\mathbf{T}_{\mathbf{F}}^{\boldsymbol{\Sigma}}$, classified also as $\alpha - \mathbf{nodes}$, from the starting point, associated with nodes $(\xi_0, \eta)$ of $\mathbf{T}_{\mathbf{F}}$,
4. compute cell by cell all the other nodes of $\mathbf{T}_{\mathbf{F}}^{\boldsymbol{\Sigma}}$, classified as $\beta - \mathbf{nodes}$, from $x_0$ and the nodes associated with nodes $(\xi, \eta_0)$ and $(\xi_0, \eta)$ of $\mathbf{T}_{\mathbf{F}}$.

The nodes of $\mathbf{T}_{\mathbf{F}}^{\boldsymbol{\Sigma}}$ associated with nodes $(\xi, \eta_0)$ and $(\xi_0, \eta)$ of $\mathbf{T}_{\mathbf{F}}$ and the $\alpha - \mathbf{nodes}$ are located on the surface along the geodesic lines emanating from the point of impact. Regarding the $\beta - \mathbf{nodes}$, various algorithms are proposed [33-34, 42]. Most of them use an analytical expression of the surface and formulate the draping problem in terms of non-linear partial differential equations. Other algorithms are also proposed to simplify these equations by using a discrete approximation of the surface by flat triangular face (i.e. a mesh of the surface). Based on this latter approach we propose a new algorithm. The $\beta - \mathbf{nodes}$ are computed by solving an optimization problem corresponding to determine a vertex of an equilateral quad plotted on the surface from the data of the three other vertices. This

optimization problem formulates the direction of the geodesic lines emanating from the searched vertex [45, 55, 57].

Consequently, two problems arise:

1. Problem 1: determine the geodetic exit of a given point of surface according to a given orientation.
2. Problem 2: determine the geodetic exits of these points intersecting itself mutually according to given two points of surface and lengths (these geodetic is given according to their orientations).

## 2.2. Numerical Examples of Geometrical Approach

Three draping simulation examples are given. These simulations are performed using the geometrical analysis computer code GeomDrap [45] and the FEA computer code Abaqus/explicit [58]. For each example, we assume that a mesh of the piece to drape is given. The first and second examples show the influence of the fibre orientations draping in the draping process. The last example shows the efficiency of the proposed method to simulate geometrically the draping of B-Pillar composite part.

The first example concerns the geometrical draping of a base plate piece. The figure 3 shows the piece as well as a mesh of this piece. The centroid of this piece is chosen as the point of impact for which two different fibre orientations (0°/90°) and $(\pm 45°)$ are specified. Figure 4 shows the resulting 3D surface lay-up for the (0°/90°) fibre orientation and the 2D corresponding flat patterns. Likewise, figure 5 shows the draping results for the $(\pm 45°)$ fibre orientation. One can notice that, in the considered cases, the surface of the piece is draped globally. However, in the second case, a smaller area of the flat fabric is used (cf. table 1). This result shows the importance of the fabric orientation in the draping process.

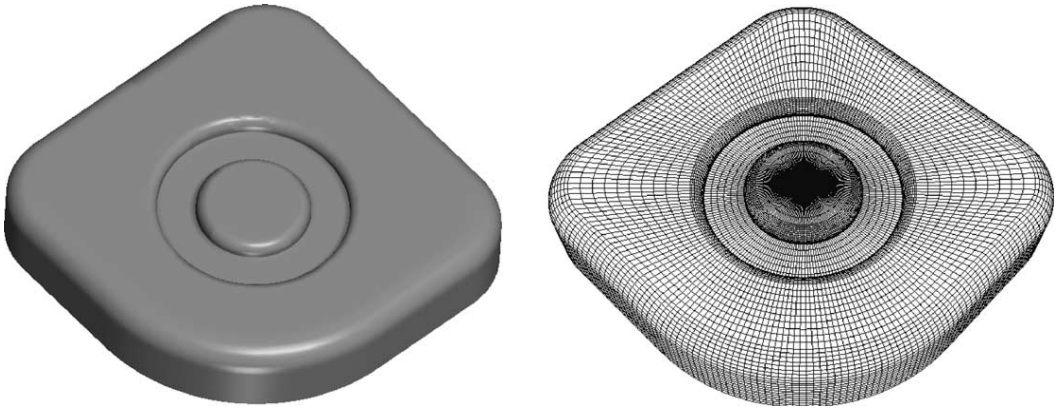

Figure 3. CAD of finite element meshing of the base plate part.

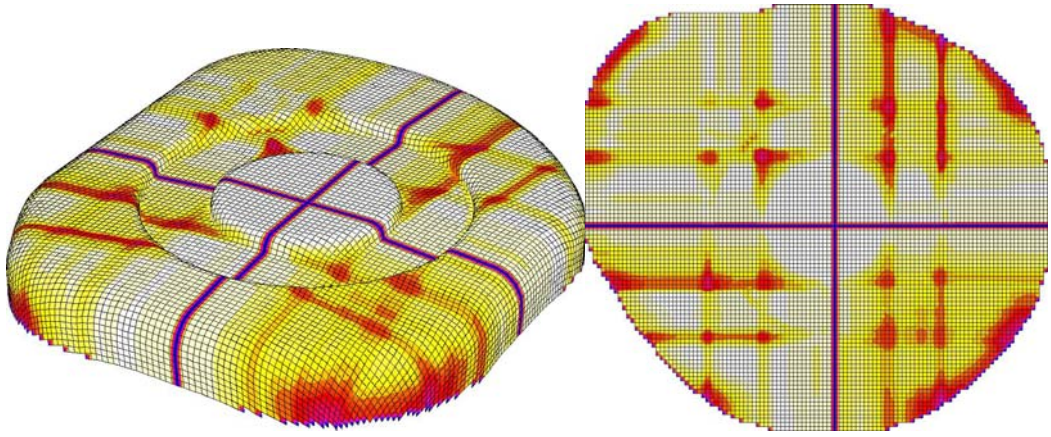

Figure 4. 3D surface lay-up (0°/90°) and 2D corresponding flat pattern.

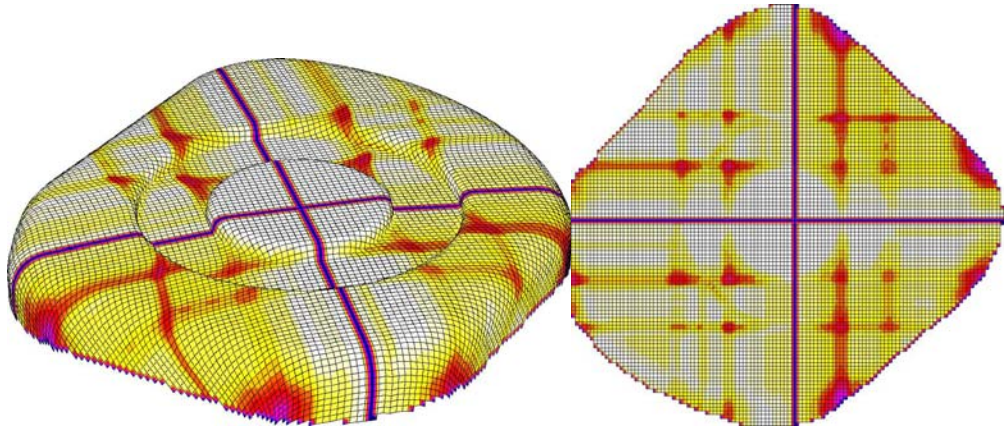

Figure 5. 3D surface lay-up (-45°/45°) and 2D corresponding flat pattern.

**Table 1. Numerical results of the geometrical draping**

| Fabric | length of fabric | drape quality | surface covering | speed grid/s | fall rate | CPU s |
|---|---|---|---|---|---|---|
| (0°/90°) | 120 | 51.0 | 96.7 % | 27494 | 19.4 % | 0.34 |
| (-45°/45°) | 120 | 58.4 | 95.2 % | 26368 | 30.8 % | 0.35 |

The second example is the draping of complex shape (car hood). The centroid of the part is chosen as the starting point from which the (0°/90°) and $(\pm 45°)$ fibre orientations are specified. Figure 6 shows the resulting 3D draping for the two orientations. We can note that all part surface is completely draped. Figure 7 presents shaded contours interpolated from the map of the fiber distortions of (0°/90°) and $(\pm 45°)$ fiber orientations. The fiber distortions for both (0°/90°) and $(\pm 45°)$ draping are very small but the maximum shear angle localization are different.

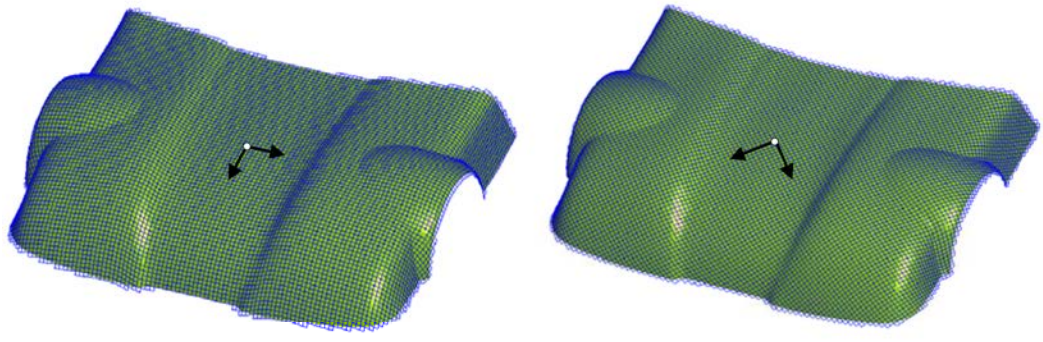

(0°/90°) (-45°/45°)

Figure 5. 3D geometrical draping of hood car part.

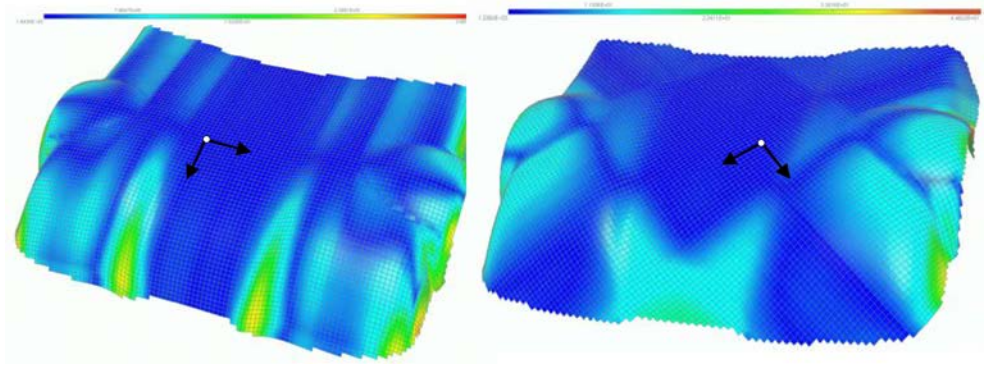

Figure 6. Iso-values of shear angles between fibres.

The last example concerns the geometrical draping of the B-Pillar composite part. The B-pillar is a major structural component for side impact car safety. The use of carbon composite as an alternative in the vehicle B-Pillar can reduce the risk of injuries on the occupant. The aim of this simulation is to demonstrate the capacity of the used model to drape completely complex shape and the effect of the chose of the starting point and the initial fibre orientation of the draping process. The centroid of the part is chosen as the starting point from which the (0°/90°) fibre orientations are specified (Figure 7a) and in order to drape completely the b-pillar shape. Figure 7b shows the resulting 3D draping corresponding to the fibre orientations. We can note that all part surface is completely draped. The fiber distortions draping are very large and the maximum shear angle localization are shown in Figure 7. The B-pillar shape is completely draped with 20689 quadrilateral elements. The choice of the starting point (impact point) has a considerable effect on draping of the part. The point optimized to drape the part completely is on the high part.

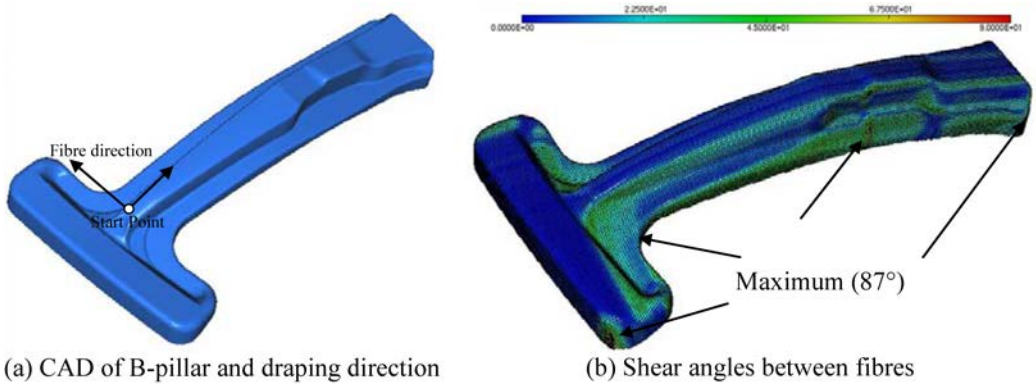


Figure 7. Geometrical draping of B-pillar composite part.

## 3. MECHANICAL APPROACH

The mechanical behaviour of composite fabrics is complex and it is a multi-scale problem due to the interactions of the fibres or yarns. The macroscopic behaviour is very much dependent on the interactions of fibres at the meso-scale (scale of the woven unit cell) and at the micro-scale (level of the fibres constituting yarns). Despite of a great amount of work in the field, there is no widely accepted model that accurately describes all the main aspects of fabric mechanical behaviour. The main model families come from the multi-scale nature of the textile.

During the forming process of woven fabric, the two main mode of deformation at the mesoscopic scale are the stretching of the fibres due fibres undulation and the in-plane shearing of the fabric resulting in a change of the angle between the warp and the left yarns. In the deep-drawing or the draping of woven fabrics, the in-plane shear of fibres is the principal mode of deformation and is very different than the sheet metal [59-65]. Figure 8 shows the evolution of two straight lines draw alternatively on warp and weft fibre directions during the forming deformation. These lines become curved but remain continuous. The absence of inter-yarn sliding ensured by the fabric weaving, viscoelastic behavior of resin and friction fiber/fiber and fiber/resin) can be observed over the main areas of the fabric (i.e. far enough from the free edges of the fabric). Also, for the composite fabrics based on high modulus, the compressive as well as bending stiffness are negligible compared to the in-plane membrane stiffness. The assumption is that each cross connection of straight warp and weft fibre before deformation remains cross connected during the deformation. The basic assumptions for the mechanical forming are that the woven fabric is considered as a continuous 3D material. The warp and weft fibres are represented by a truss which connecting points are hinged and the membrane resin is coupled kinematically to the fabric at these connecting points.

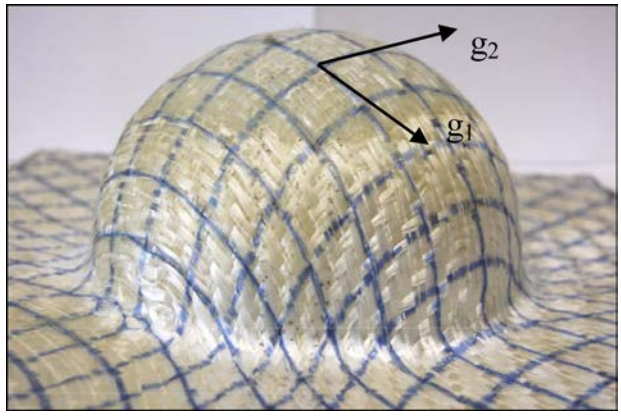


Figure 8. Woven fabric deformation mode.

## 3.1. Model Description

In the unit cell of the mesoscopic model used here for a plain-weave fabric each fibre and resin is modelled and is assumed to be a straight or a curved beam or truss. The tensile load is carried by the 3D truss or beam elements that will capture the changes in the orthotropic directions during the shearing. The 3D membrane or shell element accounts only for the shearing resistance of the fabric and hence has no tensile stiffness. The interaction warp-weft yarn and resin-fibres is negligible. In this approach, the stress and strain of a continuous material are related to fibrous reinforcement using the constitutive relation in a non-orthogonal frame directed by the fibre directions. In this study we consider two yarn directions and we use them to define the non-orthogonal frame. This approach uses the Green Naghdi frame. It is an orthonormal frame which is rotated by R, the rotation of the polar decomposition in which the local stress increment computations at finite strain are made [66-70].

Two reference frames have to be considered. The $\mathbf{e}_i$ unit vectors define the local orthogonal reference frame that rotates with the continuum material, and the $\mathbf{g}_i$ basis vectors form a non-orthogonal frame that follows the fibre direction. Here, $(\mathbf{g}_1, \mathbf{g}_2)$ correspond to warp and weft directions, respectively.In this case, for each connecting point $\vec{\mathbf{X}}^{\mathbf{f}}$ of warp and weft yarns is associated a material position space of a resin $\vec{\mathbf{X}}^{\mathbf{m}}$. At the connecting points we have $\vec{\mathbf{X}}^{\mathbf{f}} = \vec{\mathbf{X}}^{\mathbf{m}} = \vec{\mathbf{X}}$ before deformation. The current position of these points is obtained by:

$$\begin{cases} d\vec{\mathbf{x}}^{\mathbf{f}} = \mathbf{F}^{\mathbf{f}}\left(\vec{\mathbf{X}}, \mathbf{t}\right) d\vec{\mathbf{X}}^{\mathbf{f}} & \textbf{fibres} \\ d\vec{\mathbf{x}}^{\mathbf{m}} = \mathbf{F}^{\mathbf{m}}\left(\vec{\mathbf{X}}, \mathbf{t}\right) d\vec{\mathbf{X}}^{\mathbf{m}} & \textbf{resin} \end{cases} \tag{1}$$

where $\mathbf{F}^{\mathbf{f}}$ and $\mathbf{F}^{\mathbf{m}}$ are the deformation gradient tensor of fibre and resin respectively. The relationship of the no sliding inter-fibre can write at each connecting point as

$\vec{x} = \vec{x}(\vec{X}, t) / \vec{x}^{\,f} = \vec{x}^{\,m} = \vec{x}$. The gradient of transformation of the pre-impregnated woven fabric **F** and the pseudo gradient of transformation of the fibre $\mathbf{F}^f$ are defined by the function

$$\begin{cases} F_{ij}^{f} = \lambda_L g_i \otimes g_{0j} & \text{fibres} \\ F_{ij}^{m} = \dfrac{\partial \mathbf{x^m}}{\partial \mathbf{X^m}} e_{0i} \otimes e_{0j} & \text{resin} \end{cases} \tag{2}$$

where $\lambda_L^f$ is the longitudinal elongation of each fibre and $g_{0i}$ and $g_i$ are respectively the fibre orientations in the initial $C_0$ and the current $C_t$ configurations and are the resin . The relative rotation of fibre can be associated to the rotation of the rigid body of the median line of the fibre $\mathbf{R}$. We can note this assumption by the following kinematic relation:

$$\mathbf{R} = g_i \otimes g_{0i} \tag{3}$$

Using the above assumptions, the mechanical deformation of composite fabric depends on the relative movement of fibres and the deformation of not polymerized resin.

$$\begin{cases} \lambda_i^f = \sqrt{g_{0i} F^{fT} F^f g_{0i}^f} & \text{fibres} \\ U^m = \sqrt{F^{mT} F^m} & \text{resin} \end{cases} \tag{4}$$

The shaping problem imposes the use of incremental formulation in finite deformations. In finite deformation analysis a careful distinction has to be made between the coordinate systems that can be chosen to describe the behaviour of the body. The rate constitutive equations for finite strain use objective derivatives [65-66]. The problem of the integration of strain rate tensors is a central one in large deformations. The rate of deformation tensor of woven fabric is obtained by:

$$\begin{cases} D^f = \left( \dfrac{\dot{\lambda}_i^f}{\lambda_i^f} \right) \left( g_i \otimes g_i \right) & \text{fibres} \\ D^m = \dfrac{1}{2} \left( \dot{F} F^{-1} + F^{-T} \dot{F}^T \right) \left( e_{0i} \otimes e_{0i} \right) & \text{resin} \end{cases} \tag{5}$$

The rate equations for finite strains use objective derivatives [36-38, 66]. The approaches traditionally developed in finite element codes for anisotropic metal at large strains are based on Jaumann corotational formulation or the Green–Naghdi approach. In these models, a rotation is used both to define an objective derivative for the hypoelastic model law and to update the orthotropic frame. The rotations used in Green–Naghdi and Jaumann derivatives are average rotations of the material (polar rotation and corotational rotations respectively). The frame associated with Green-Naghdi's derivative is defined, at the material point

considered. The rotation $\mathbf{R}^f$ is used to update the initial constitutive axes of warps or weft fibres $g_{0i} \otimes g_{0i}$ to the current constitutive axes and the rotation $\mathbf{R}$ is used to update the initial constitutive axes of resin $e_{0i} \otimes e_{0i}$. The stretching tensors Eq. (5) are written in the rigid body rotation frames. The longitudinal component is $\overline{D}_L^f = \dot{\lambda}_L^f / \lambda_L^f$ and the transversal components $\left(\overline{D}_T^f, \overline{D}_3^f\right)$ are obtained by the unidirectional behaviour of fibre as $\overline{D}_T^{fR} = \overline{D}_3^{fR} = -\nu_{LT}\overline{D}_L^{fR} \Rightarrow \lambda_T^f = \lambda_3^f = \left(\lambda_L^f\right)^{-\nu_{LT}}$ and $\nu_{LT}$ is the Poison's ratio of fibre. Using Green-Naghdi's objective tensor stress, the stress rate $\overline{\sigma}_L^f$, depending on the stretching deformation $\overline{D}_L^f$, and the stress rate tensor of the membrane resin $\overline{\boldsymbol{\sigma}}^m$, depending on the tensor deformation rate $\overline{\mathbf{D}}^m$ and the elastic properties $\mathbf{C}^m$, can be written at each time as: The stress and strain relationship of the woven fabric composites are defined in the non-orthogonal material coordinate frame. Therefore, coordinate transformations of stress and strain into the orthogonal coordinate system should be considered in the non-orthogonal constitutive model as $\sigma = \overline{\sigma}^f + \overline{\sigma}^m$:

$$\sigma = \begin{pmatrix} \sum_{weft} E_L^f(\lambda_1^f)\frac{\dot{\lambda}_1^f}{\lambda_1^f} - \nu_{LT}E_L^f(\lambda_2^f)\sum_{weft}\frac{\dot{\lambda}_2^f}{\lambda_2^f} & 0 & 0 \\ 0 & \sum_{warp} E_L^f\left(\lambda_2^f\right)\frac{\dot{\lambda}_2^f}{\lambda_2^f} - \nu_{LT}\sum_{weft} E_L^f(\lambda_1^f)\frac{\dot{\lambda}_1^f}{\lambda_1^f} & 0 \\ 0 & 0 & 0 \end{pmatrix} + \begin{pmatrix} \frac{E^m}{1-\nu_m{}^2} & \frac{\nu_m E^m}{1-\nu_m{}^2} & 0 \\ \frac{\nu_m E^m}{1-\nu_m{}^2} & \frac{E^m}{1-\nu_m{}^2} & 0 \\ 0 & 0 & G^m \end{pmatrix} \begin{Bmatrix} \overline{D}_{11}^m \\ \overline{D}_{22}^m \\ \overline{D}_{12}^m \end{Bmatrix} \tag{6}$$

The constitutive law of fibres is nonlinear and is written in terms of longitudinal modulus of stretching $E_L^f\left(\lambda_L^f\right)$, the compressive stiffness $\left(\lambda_L^f \le 0\right)$ of fiber is supposed negligible $E_L^f = 0$. Later is function of elongation of warp and weft fibre $\left(\lambda_1^f, \lambda_2^f\right)$, effective elastic modulus of fibre $\overline{E}_f$ and undulation factor $\varepsilon_{sh}$; $\left(E^m, \nu_m\right)$ are the membrane elastic properties. To determine the stress state in a membrane material at a given time, the deformation history must be considered. For linear viscoelastic materials, a superposition of hereditary integrals describes the time dependent response. Let $G^m(t)$ be the shear stress relaxation modulus of the not polymerized resin and $G^{m^\infty} = G^m(t = \infty)$ the limit value. The viscoelastic behaviour of not polymerized resin is formulated in the time domain by the hereditary integral and using the relaxation time $\tau_k$ and the shear modulus relaxation, which are material parameters $G^{m^k}$. Hereditary integrals with Prony series kernels can be applied to model the shear behavior of the not polymerized resin (Abaqus 2004). The behavior of fibre and resin can be written as:

$$\begin{cases} E_L^f\left(\lambda_L^f\right) = \overline{E}_f\left(1 - \mathrm{Exp}\left(\dfrac{-\dot{\lambda}_L^f}{\lambda_L^f \varepsilon_{sh}}\right)\right) & \text{fibres} \\ G^m(t) = G^m(\infty) + \sum_1^k G^{m^k}\,\mathrm{Exp}\left(\dfrac{-t}{\tau_k}\right) & \text{resin} \end{cases} \tag{7}$$

## 3.2. Finite Element Formulation

Each material point is moving as in a continuum, ensured by the non-sliding of fibers due to fabric weaving and resin behavior. Therefore, a nodal approximation for the displacement can be used. The deformation of composite fabric is described within the frame of membrane assumptions. The energy of deformation $\Pi(\dot{\mathbf{u}})$ is obtained by a summation of membrane strain energy of not polymerized resin and elastic tensile strain energy of fibers:

$$\delta\Pi(\dot{u}) = h_0 \int_{S_0^m} \overline{\sigma}^m : \delta\overline{D}^m ds + \sum_{\text{fibres}} S_0^f \int_{L^f} \overline{\sigma}_L^f : \delta\overline{D}_L^f dl - \int_{\Gamma_\sigma} \overline{t}.\delta\dot{u} d\Gamma \tag{8}$$

where $h_0$ denote the initial thickness of fabric, $L^f$ the length of fiber and $S_0^f$ the initial effective cross section of fibre and $\overline{t}$ is the external surface load applied along $\Gamma_\sigma$ of woven fabric. The effective cross section of the fibre $S_0^f$ and the effective surface $S_0^m$ of the membrane resin, that assumed no void between the fibre and the resin, was used are calculated by using the fibre volume fraction $V_f$ of the woven fabric $(V_{fabric} = V_f S_0^f L^f + (1 - V_f) h_0 S_0^m)$.

The global equilibrium of the fabric is obtained by minimizing the total potential energy $\Pi(\dot{u})$. The effect of spatial equilibrium of composite material on the actual configuration is established in terms of nonlinear equations: kinematic non-linearity, material non-linearity and contact with friction non-linearity. It is linearized for each load increment by an iterative Newton method. It should be emphasized that during the motion, nodes and elements are permanently attached to the material points with which they were initially associated. Consequently, the subsequent motion is fully described in terms of the current nodal positions as:

$$x = \sum_{k=1}^{m} N^k(\xi,\eta) X^k + \sum_{k=1}^{m} N^k(\xi,\eta) u^k \tag{9}$$

where $u^k$ are the nodal displacements of each connecting point, $N^k(\xi,\eta)$ are the standard shape functions (of membrane of truss element) and (m) denotes the number of nodes.

The discretization of rate deformation tensor can be obtained by introducing Eq.5 into the definition of ( $\overline{D}_L^f$ and $\overline{\mathbf{D}}^m$ ) and given in Eq. 8 to give:

$$\begin{cases} \bar{D}_L^f = \dfrac{\dot{\lambda}_L^f}{\lambda_L^f} = \dfrac{1}{\alpha_n^2}\left(\dfrac{dx^T}{d\xi}\dfrac{d\dot{u}}{d\xi}\right) = \left[B_{fibres}\right]\dot{u}_n & \text{fibres} \\ \bar{D}^m = \dfrac{1}{2}R^T\left(\dfrac{d\dot{u}}{d\xi}\dfrac{d\xi}{dx} + \dfrac{\partial\dot{u}^T}{d\xi}\dfrac{d\xi}{dx}\right)R = \left[B_{resin}\right]\dot{u}_n & \text{resin} \end{cases} \tag{10}$$

where $\alpha_n = \sqrt{\dfrac{d\mathbf{X}^{fT}}{d\xi}\dfrac{d\mathbf{X}^{f}}{d\xi} + 2\dfrac{d\mathbf{X}^{fT}}{d\xi}\dfrac{d\mathbf{u}}{d\xi} + \dfrac{d\mathbf{u}^T}{d\xi}\dfrac{d\mathbf{u}}{d\xi}}$ and $\left[B_{resin}^e\right]$ and $\left[B_{fibres}^e\right]$ are the geometric or strain-displacement matrix of membrane resin and truss fibres.

In a finite element approximation, the only independent variables in the equations of linearized virtual work are the displacements of the material points. Substituting the element coordinate and displacement interpolations into the equilibrium equations, for a given set of elements we obtain the state that forces acting on a fabric equals the mass times the acceleration of the body:

$$\sum_e \left[M^e\right]\{\ddot{u}\} + \sum_e \left(\left\{\Re_{int}^e\right\} - \left\{\Re_{ext}^e\right\}\right) = \{0\} \tag{11}$$

where $\left[\mathbf{M}^e\right]$ is the consistent composite mass matrix and $\left(\left\{\Re_{int}^e\right\} - \left\{\Re_{ext}^e\right\}\right)$ is the so called quasi-static equilibrium residual :

$$\begin{cases} \left[M^e\right] = \rho_r h_0 \int_{S^m} \left[N^e\right]^T\left[N^e\right]ds + \sum_{fibres} \rho_f S_0^f \int_L \left[\tilde{N}^e\right]^T\left[\tilde{N}^e\right]dl \\ \left\{\Re_{int}^e\right\} - \left\{\Re_{ext}^e\right\} = h_0 \int_{S^m} \left[B_{resin}^e\right]^T\left\{\bar{\sigma}^{mR}\right\}ds - \sum_{fibres} S_0^f \int_{L^f} \bar{E}_L^f \left[B_{fibres}^e\right]^T\left\{\bar{\sigma}^{fR}\right\}dl - \int_{\Gamma_f} \left[N^e\right]^T\left\{\bar{t}\right\}ds \end{cases} \tag{12}$$

where $\left[N^e\right]$ and $\left[\tilde{N}^e\right]$ are the matrix of the nodal interpolation functions both associated elements and $\left(h_0, S_0^f\right)$ are the initial thickness and surface of resin and fibres, respectively. The index e refers to the $e^{th}$ element.

According to the different modes of deformation occurring in the prepreg fabric during the shaping process, bi-component finite elements are developed to characterize the mechanical behavior of thin composite structures. The bi-component element is based on an association of 3D linear membrane finite elements (T3 and Q4) combined with a complementary truss linear finite elements. The global stiffness of composite fabric is obtained by the summation of elementary stiffness matrix of warp fiber, elementary stiffness matrix of weft fiber and elementary stiffness matrix of resin. These finite elements are complementary in the finite element discretization (isoparametric and use three DOF per node) and use the same mechanical formulation in finite deformations (Green- Naghdi's

approach). The non linear constitutive equation of fibre behavior is implemented in the Abaqus/Explicit using VUMAT user's subroutine [17-20].

The governing equilibrium Eq. 11 is solved as a dynamic problem using explicit integration. This is achieved by using the central difference method to approximate the velocity and the acceleration in the next time step, using only information from the previous step, where all state variables are known. This approach has proven to be, in particular, suitable to highly non-linear geometric and material problems, particularly where a large amount of contact between different structural parts occurs. In the present work, the Dynamic Explicit (DE) resolution procedure is used within the general purpose FE code Abaqus/Explicit. The DE algorithm available in Abaqus/Explicit for solving the algebraic system works by using the lumped form of the mass matrix [58, 66]. The major disadvantage of the explicit scheme is that it is only stable for time steps small enough. This can cause for instance the energy balance to be changed. One simple and conservative criteria for a stable time increment:

$$t_{stable} = \frac{\rho_r L^e}{\bar{E}^f} \tag{13}$$

where $L^e$ is the minimal length of membrane element, $\rho_r$ the resin density and $\bar{E}^f$ Young's modulus of fibre. The interpretation of this requirement is that the time increment must be shorter than the time it takes for a propagating wave in the material to cross the shortest side of an element. Thus, the element size and the critical time increment are connected. The smaller the elements are, the shorter the time increment must be. Because of the difference in wave speed for different materials, the critical element size is larger for a stiff material (e.g. steel) than for a softer material (e.g. polymer).

## 3.3. Application of Mechanical Approach

### *3.3.1. Uniaxial Test*

Due to the importance of the composite fabric behaviour on material formability, tensile test of pre-impregnated fabric is proposed in order to study the influence of fibre orientation, fibre undulations due to fabric weaving and resin behaviour. At processing, the impregnated fabric is idealised as a viscous material subject to the kinematic constraints of incompressibility and inextensibility in the fibre direction. The pre-impregnated fabric tested in this study was a satin 5 with aramid woven fabric. The fabric was impregnated with epoxy resin using a hot-melt pre-pregging process (the mechanical properties are given in Table 2). A lower loading velocity will generate lower viscous forces at the intra-ply shearing of fabric. In this experiment, a displacement in the vertical direction is imposed at the moving extremity of the rectangular composite specimen with three layers of fibres (length =150mm and width=30mm and thickness=2mm). The uniaxial tensile test (see Figure 9) is carried out for different orientations of fibres with the loading direction (0, 15, 30 and 45°). The experimental effort imposed by the tensile machine is compared to the numerical values for different fibre orientations in Figure 10. The behaviour of the not polymerized resin and the

initial fibre orientation influenced largely the global response of the fabric during tensile loading. In this figure we can show the good correlation between the model and the experimental results. The agreement between predicted and experimental values is good and proves the validity of the proposed model of pre-impregnated woven fabric behaviour. The numerical model described above clearly shows the strong non linearity of this behaviour law. It takes into account the mechanical characteristics of a viscoelastic resin, the anisotropic behaviour of fabric and the geometrical non linearities due to the high deformability of fibres (straightening and relative rotation).

**Table 2. Mechanical properties of the pre-impregnated composite fabric**

| $E_f$ (MPa) | $\varepsilon_{sh}$ | $\rho$ (g/cm$^3$) | | | | |
|---|---|---|---|---|---|---|
| 130000 | 0.005 | 1,45 | | | | |
| time **(s)** | 0.01 | 0.1 | 1 | 10 | 100 | 1000 |
| Shear modulus of resin $G^{m^k}$ | 0.02332 | 0.023332 | 0.083509 | 0.11723 | 0.14423 | 0.178 |

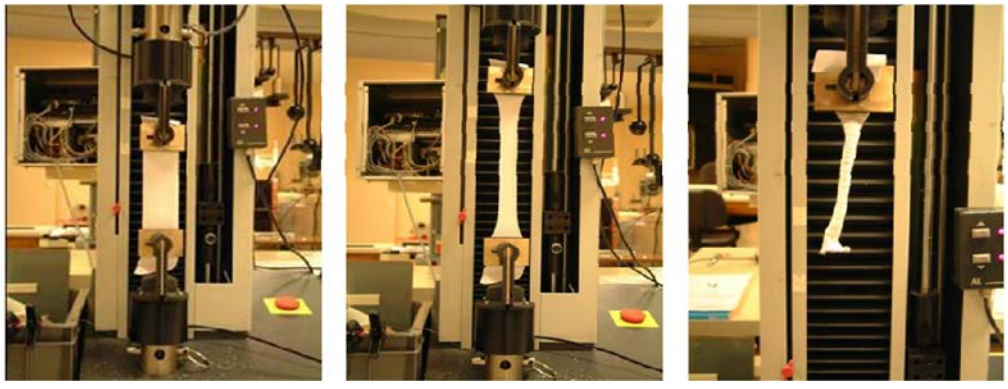

Figure 9. Tensile apparatus of pre-impregnated composite fabric specimen.

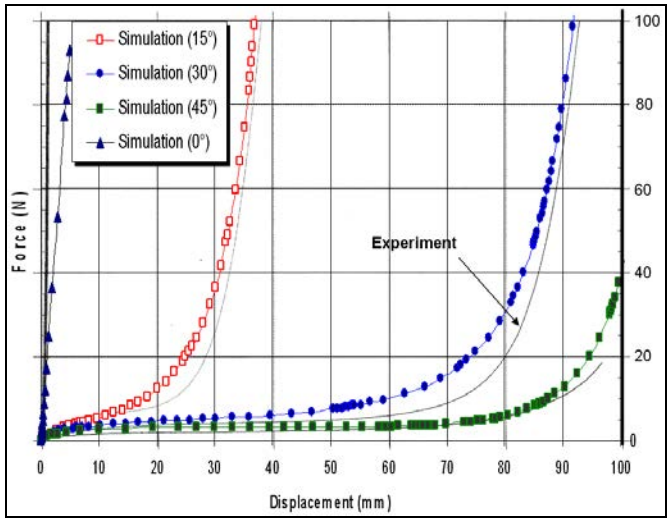


Figure 10. Load force- displacement of the fabric specimen for different fibre orientations.

### *3.3.2. Biaxial Test*

In order to determine and analyse the undulation and interaction effects, a biaxial tensile apparatus has been built in order to test woven materials in both the warp and weft directions. The loads are measured using load cells located very close to the specimen in order to avoid the influence of friction within the device. The strains are measured using extensometers devices which permit the verification of the homogeneity of the strain field in the effective part of the specimen. The set of tests which have been performed on different fibre fabrics (carbon twill 2x2), mainly used in aeronautics, has shown features of the biaxial behaviour and the importance of the undulations due to the weaving. For a given fabric, the response is strongly influenced by the strain ratio in warp and weft directions due to large fibre undulations [46]. Especially, the non-linearity in warp and weft direction is increasing. The tendency of the fibre to straighten is more impeded when the strain in the perpendicular direction is large (see Table 3). The biaxial specimen, as shown in Figure 11, was modelled in 2D with 400 four nodes membrane elements (representative of elastic behaviour of not polymerized matrix) and 1600 two nodes truss elements (representative of elastic non linear behaviour of fibres) of Abaqus element library. The load was applied at the same time on each strip. The overall agreement of the proposed non-linear numerical model is very good in comparison with the experimental results (see Figure 12).

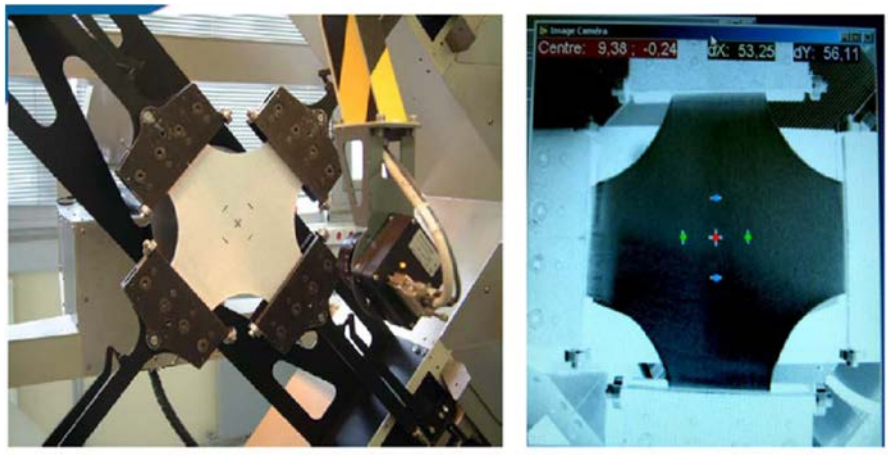


**Figure 11.** Device for a biaxial tensile test on cross fabric specimen.

**Table 3. Mechanical parameters of the composite fabric carbon twill 2x2**

| | Warp direction | Weft direction |
|---|---|---|
| Maxi strain | 132% | 80% |
| Maxi displacement | 80 mm | 80 mm |
| Maxi force | 620 N | 1180 N |
| Maxi Stress | 35.42 MPa | 67.42 MPa |
| Longitudinal Young's modulus $\left(\overline{E}_f\right)$ | 15.72 MPa | 27.79 MPa |
| Undulation factor $\varepsilon_{sh}$ | 0.015 | 0.20 |

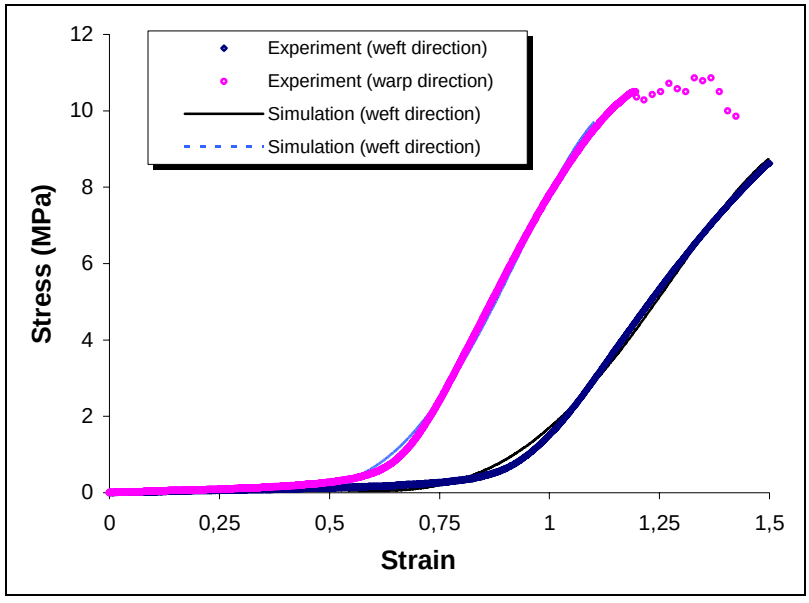


Figure 12. Effect of the fibre undulation of the force versus displacement response.

### *3.2.4. Deep-Drawing of Prepreg Woven Fabric*

The numerical analysis of prepreg composite fabric deformation by deep-drawing process is performed by utilizing the commercial FEM-package ABAQUS/EXPLICIT. The resin is modeled by using 1600 membrane finite elements (linear triangular element M3D3) and warp and weft fibres are modeled by 3200 truss finite elements (linear element T3D2). The rigid surface is modeled by 1600 Bezier patches (three nodes R3D3 and four nodes R3D4). The behavior of the resin is assumed to be isotropic viscoelastic and the behaviour of the fibre is supposed as elastic.

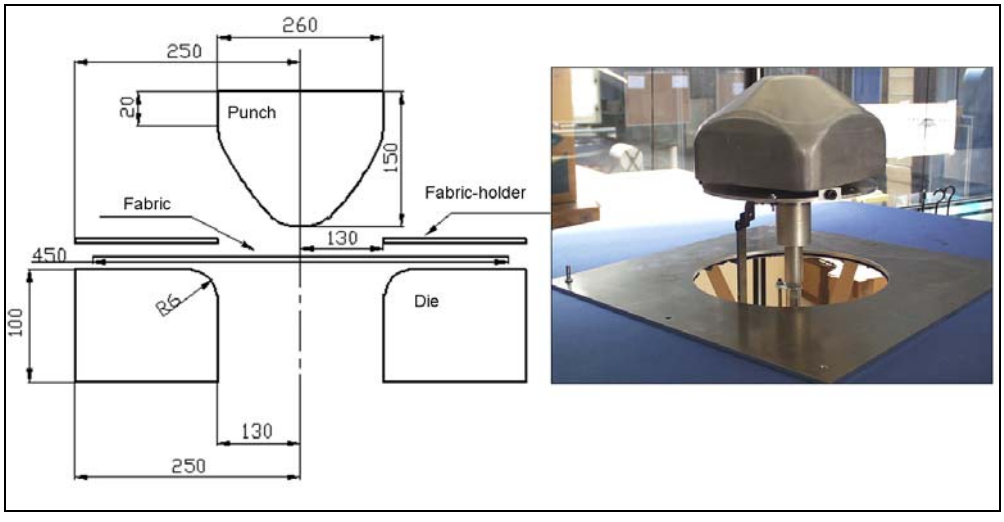


Figure 13. Geometry of deep-drawing tools.

The first forming example concerns the 3D deep-drawing of aramid pre-impregnated fabric with conical tools (see Figure 13). The mechanical properties of the used material are given in Table 2. Figure 14 reports the experimentally obtained shapes with respect to 0°/90° and $\pm 45°$ fibre orientation for different punch displacements (initial, and final for 100mm of punch displacement). The corresponding final computed shapes are shown in Figure 15. The evolution of the predicted shear angle variations mechanical approach is compared on Figure 16 with the experimental values. We notice that these shear angle values are very large >38° for mechanical approach along the median line for $\pm 45°$ fabric and along the diagonal line for 0°/90° fabric. But along the median lines of 0°/90° and along the diagonal lines of $\pm 45°$ the angular distorsions are very small <6°.

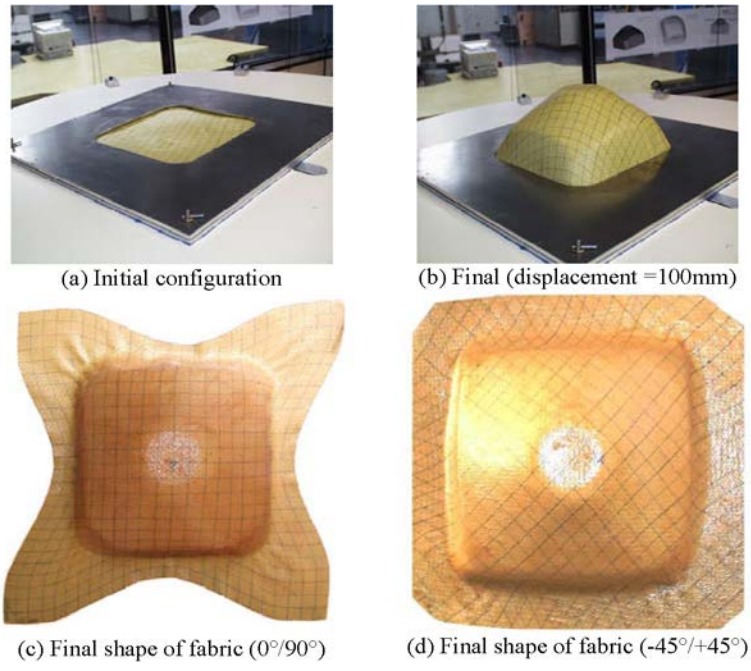


Figure 14. Experimental results (a) (0°/90°) and (b) (-45°/45°).

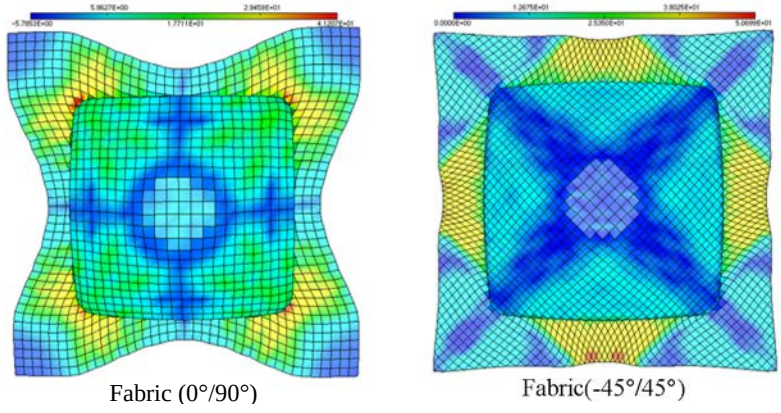


Figure 15. Predicted results (a) (0°/90°) and (b) (-45°/45°).

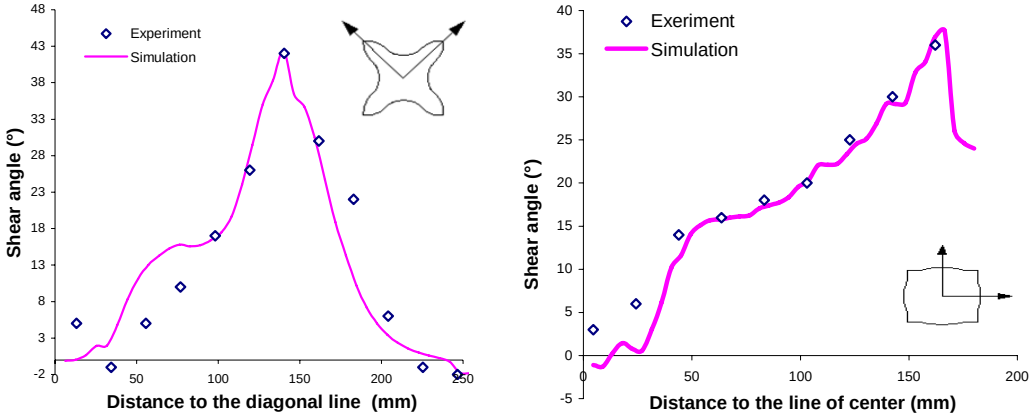


Figure 16. A comparison between experimental and predicted shear angles.

### *3.2.5. Deep-Drawing of Dry Woven Fabric*

The second example is the 3D deep-drawing of dry glass woven fabric by hemispherical punch by experimental and mechanical approaches. The initial shape of the glass fibre fabric is a square (360x360mm). Its edges are free but a pressure equal to 2MPa is applied on the binder and the friction coefficient between the glass fabric and the steel tools is 0.27. The forming simulation has been performed in ABAQUS/Explicit using rigid tools. As mentioned before the shear resistance model is assigned to reduced membrane elements, and truss elements parallel to the membrane edges represent the high tensile stiffness in the yarn direction. Figures 17a and 18a report respectively the experimental obtained shapes with respect to (0°/90°) and $(\pm 45°)$ fibre orientations, while figures 17b and 18b show the final shape using the numerical approach. Likewise, the numerical simulation agrees with the experimental results. The angular fibre distorsion exceeds 38° along the diagonal axis for (0°/90°) fibre orientations and 50° along the diagonal axis for $(\pm 45°)$ fibre orientations. Furthermore we can notice that the final shape obtained with (0°/90°) fibre direction is very different from the (-45°/+45°). Another interesting result of the numerical calculation is the angular distortion variations between warp and weft fibres.

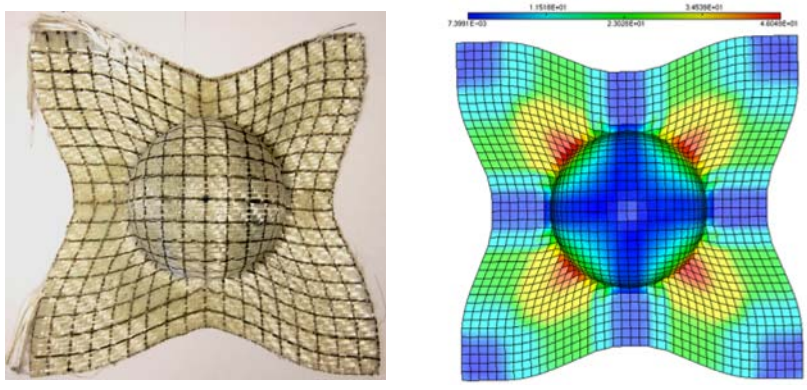

Figure 17. A comparison between (a) experimental and (b) predicted shape shear angles of (0°/90°).

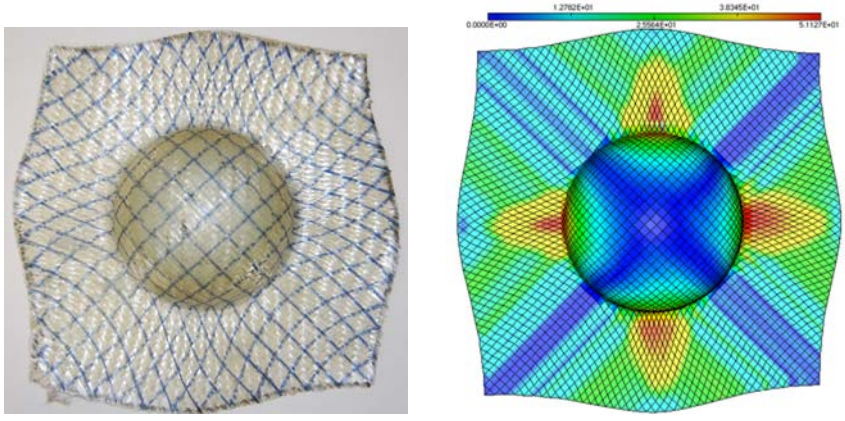

Figure 18. A comparison between (a) experimental and (b) predicted shape and shear angles of $(\pm 45°)$.

## 4. REMESHING PROCEDURE OF COMPOSITE FABRIC

The shape of elements in the finite element analysis may be the most important of many factors which induce a discretizing error. In particular, the efficiency of adaptive refinement analysis depends on the shape of the elements, and so estimating the quality of element shape is requisite during the adaptive analysis being performed. Unfortunately, most posterior error estimates can not evaluate the shape error of an element, so that some difficulties remain in the application of an adaptive analysis. The goal of this section is to develop a fully automatic procedure to update the geometry of the deformed fabric and generate its discretization in an effort to develop an automated modeling system for forming analyses. There are several key technical issues that affect the overall accuracy of the simulation that must be considered in the automation of the process. The use of finite element methods for problems where the domain evolves during the simulation presents a number of challenges that are not present in solutions for a fixed domain. Two high level issues that must be considered when automating process simulations (i) *when* to remesh, and, (ii) *how* to remesh.

The criteria used to trigger a remesh are collectively called the *remeshing criteria*. Four sources of errors that influence the decision to remesh are:

(i) Geometric approximation errors (due the discretization of the workpiece and the tools)
(ii) Element distortion errors (error due to element shape).
(iii) Mesh discretization errors (errors in the solution due to use of specific basis functions on individual finite elements).
(iv) Mesh rezoning errors (an issue critical to the successful use of remeshing in history dependent solution procedures is the transfer of the appropriate solution variables between meshes.).

The impact of the different types of errors encountered based on metrics to measure them will key a remeshing step. The process of remeshing focuses on controlling these errors so

that the simulation can continue. The objective of the geometry update procedure is to take a finite element mesh representing the current state of the workpiece, and evolve the geometric representation of the workpiece to represent its current deformed shape. This geometric representation is then discretized to generate a mesh consisting of valid, high quality elements focused on controlling the mesh discretization and distortion errors [71-76]

The simulation of the composite fabric forming is based on an iterative process. At first, a coarse initial mesh of the part is generated with bi-component finite elements (quadrilateral element representing the resin behavior and truss elements representing the fiber behavior). At each step, a finite element computation is realized in order to simulate numerically the composite forming process for a small tools displacement [52, 55, 63]. Then, the remeshing is applied after each deformation increment, if necessary, according to the following scheme:

(i) Definition of a physical size map based on the adaptation of the mesh element size with respect to one of the mechanical fields,
(ii) Definition of a geometrical size map based on the geometric curvature of the boundary,
(iii) Adaptive remeshing of the domain based on refinement and coarsening techniques with respect to the physical and geometrical sizes map.

## 4.1. Definition of a Physical Size Map

A physical size map is defined by calculating a physical size ($h_D$) for each element of the part. This physical size is defined with respect of one of the mechanical field. A critical value has been defined from which the minimal size must be reached. For the other elements, a linear size variation can be used. For a given element, if the ratio between the average size of its edges ($\overline{h}$) and its physical size ($h_D$) is greater than a given threshold, the element must be refined. During the step of remeshing, the refinement is repeated as long as the physical size is not reached.

## 4.3. Definition of a Geometrical Size Map

The geometrical size map indicates if a boundary membrane element must be refined or not. The geometric curvature is estimated at each boundary vertex of the domain. If this curvature has been modified during the deformation of the computational domain, all elements sharing this boundary vertex must be refined. At each iteration load the “curved” elements are identified using a geometrical criterion which, for a given element, represents the maximal angular gap between the normal to the element and the normals at its vertices. An element is thus considered to be “curved” if the corresponding angular gap is greater than a given threshold (for example 8 degrees). The normal vector $\vec{\nu}$ at a node P can be defined as the normalized average of the unit normal vectors $\vec{N}_i$ ($i$=1,..$m$) to elements sharing node P.

$$\vec{v} = \frac{\sum_{i=0}^{m} \vec{N}_i}{\left\| \sum_{i=0}^{m} \vec{N}_i \right\|} \tag{14}$$

The computation of normal vector to the element depends on the element shape (triangle or quadrilateral) and on the element type (ordinary or extraordinary). The normal vector $\vec{N}$ to an ordinary triangle $P_1P_2P_3$ is the unit normal vector to its supporting plan:

$$\vec{N} = \frac{\overrightarrow{P_1P_2} \wedge \overrightarrow{P_2P_3}}{\left\| \overrightarrow{P_1P_2} \wedge \overrightarrow{P_2P_3} \right\|} \tag{15}$$

The normal vector to an extraordinary triangle is the average of the normal vectors to its two subdividing triangles.

In order to avoid the creation of poor shaped triangles, the shape quality of triangles resulting from the subdivision of each extraordinary element is considered during the refinement operation. If one of the triangle qualities is smaller than a given threshold, the extraordinary element is subdivided in four ordinary elements. The quality $Q$ of a given triangle can be defined by the following formula:

$$Q = \alpha \frac{\left\| \overrightarrow{P_1P_2} \wedge \overrightarrow{P_1P_3} \right\|}{\overline{P_1P_2}^2 + \overline{P_1P_3}^2 + \overline{P_2P_3}^2} \tag{16}$$

where $\alpha$ = 3.4641002 is a normalization coefficient in order to obtain a shape quality equal to 1 for an equilateral triangle.

A quadrilateral element is geometrically distorted if its vertices are not coplanar. To measure the distortion, we can consider the angle between the two triangles constituting the quadrilateral element. In fact, there are two possibilities to define this pair of triangles according to the cutting diagonal. Actually, we consider that a quadrilateral element is distorted if one of these angles is smaller than 145°. In this case, the quadrilateral element is subdivided by its two defining triangles. Such element is curved and its size is almost minimal.

## 4.3. Adaptive Remeshing Based on Refinement and Coarsening Techniques

The adaptive remeshing technique consists in improving the mesh by coarsening and refinement methods in order to conform to the geometry of membrane and truss elements and the mechanical fields of the current part surface during deformation. Two consecutive steps are executed:

(i) Coarsening step during which the mesh is coarsened with respect to the physical size map,
(ii) Refinement step during which the mesh is refined according to the geometrical size map and then to the physical size map
(iii) Define the deformed truss finite elements representing the fixed warp and weft fibres discretization.
(iv) Transfer the mechanical field of resin and fibres from the old mesh to the new mesh.

The refinement technique consists in a uniform subdivision into four new elements. Each triangular or quadrilateral membrane element which needs to be refined is subdivided in four. Truss linear elements associated to the refined membrane element are subdivided in two new truss elements. This procedure allows conserving the fibres orientation during the remeshing (Figure 19). An element is refined if it is a boundary element which needs to be refined (element which belongs to the list of the geometrical size map) or if its size is greater than its physical size (physical size map). There is only one element subdivision which allows preserving the element shape quality: the uniform subdivision into four new elements. For this subdivision, a node is added is the middle of each edge of the element. Boundary elements which belong to the geometrical size map are first refined. The refinement is then applied according to the physical size map. In this case, the refinement procedure is repeated as long as the physical size map is not reached. After each refinement procedure (geometrical criterion or physical criterion), an iterative refinement to restore mesh conformity is necessary. Indeed, after applying the subdivision according to the geometrical or physical criteria, adjacent elements to subdivided elements must be modified. A procedure of subdivision has been proposed for the adjacent elements in order to stop the propagation of the homothetic subdivision (see [55] for more information).

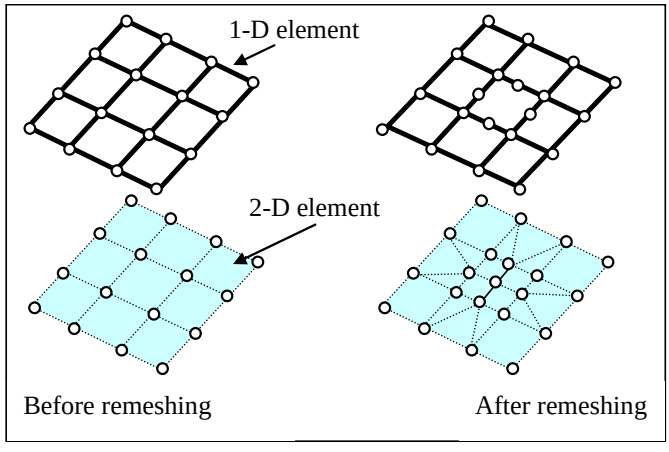


Figure 19. Remeshing of associated membrane and truss finite elements.

## 4.4. Numerical Application of Remeshing Procedure

The initial coarse mesh of the membrane resin is composed by 900 quadrilateral membrane elements representative of not polymerized matrix (930 truss element

representative of weft fibre and 930 truss element representative of warp fibre), this mesh is refined in the curved areas resulting from the deep-drawing process. The minimal element size $h_{min}$=1mm and the angular geometrical threshold is 3°. The contour of the final shape after deformation is in good agreement with the experimental results. We can see that, the initial thin fabric is computed using an initial coarse mesh, the mesh is again refined uniformly and the adaptive mesh refinement procedure is activated where elements are created automatically in regions of large curvature to even more accurately represent the complex material flow (large stretching) around the die radius. Figure 10 show the final shape draping of conical part using the geometrical approach. One can notice that, in the considered cases (0°/90°) and (-45°/45°), the surface of the conical piece is draped globally (cf. Table 2).

#### *4.4.1. Pressure Burst Tester*

The burst tester is designed for measuring the bursting strength of sample materials subjected to an increasing hydrostatic pressure. This pressure is applied to a circular region of the specimen via an elastic diaphragm. The specimen is firmly held round the edge of this circular region by a pneumatic clamping device. When the pressure is applied, the specimen deforms together with the diaphragm. This method is used to determine the pressure required to burst a textile fabric. The experimental test is carried out in IFTH laboratory. The geometry of the tool and the deformed fabric is illustrated in Figure 20. The used balanced textile fabric (jersey) consisted of 77% polyamide fibres and 26% membrane elastane. The mechanical properties of the used fabric are given in [46]. The proposed remeshing approach is used to simulate the bursting of the fabric for 52mm of punch displacement. Numerical simulations obtained with adaptive remeshing are shown in Figure 21 for different remeshing steps corresponding to punch displacement u = 24, 36, 48 and 52mm. We can see that, the initial membrane resin is computed using an initial coarse mesh (400 membrane elements), the mesh is again refined uniformly and the adaptive mesh refinement procedure is activated where elements are created automatically in regions of large curvature to even more accurately represent the complex material flow (large stretching) around the punch radii. The final mesh of the resin has 12468 T3 elements and 12216 Q4 elements. The bursting load prediction versus the punch displacement is compared with the experimental results in Figure 22. The maximum force (80kN) and the displacement (65mm) corresponding to the initiation and the propagation of the damage inside the fabric. Good agreement between the predicted results and the experimental values. Noting that, the remeshing procedure improves the predicted results in comparison with the experimental values.

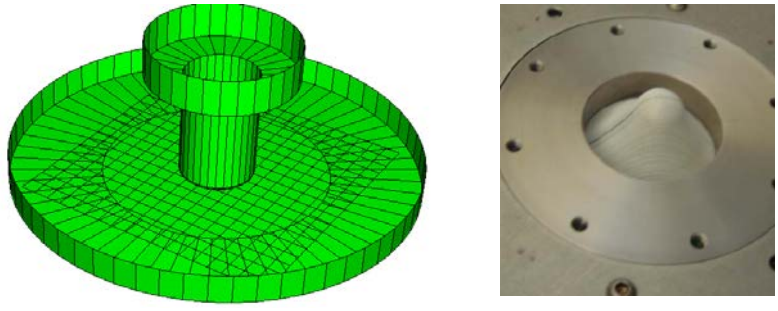

Figure 20. Geometry of textile burst and experimental test.

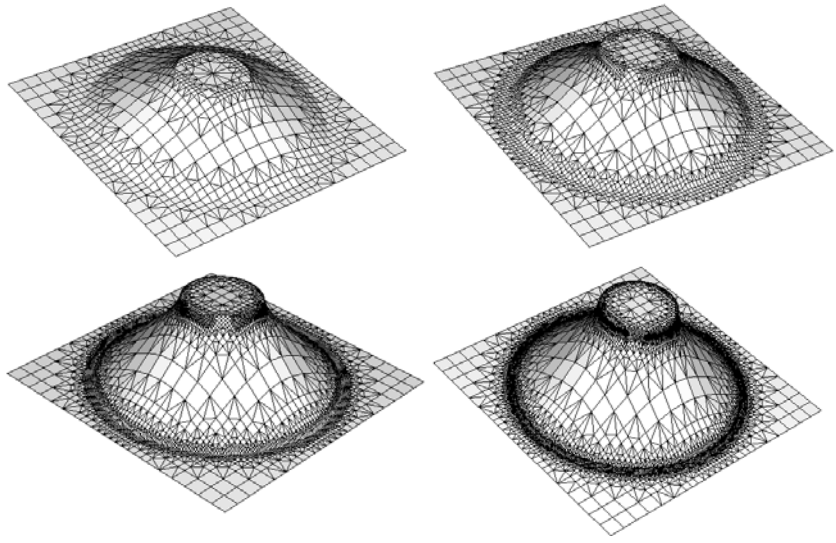

Figure 21. Fabric mesh at different punch displacement (24, 36, 48 and 52mm).

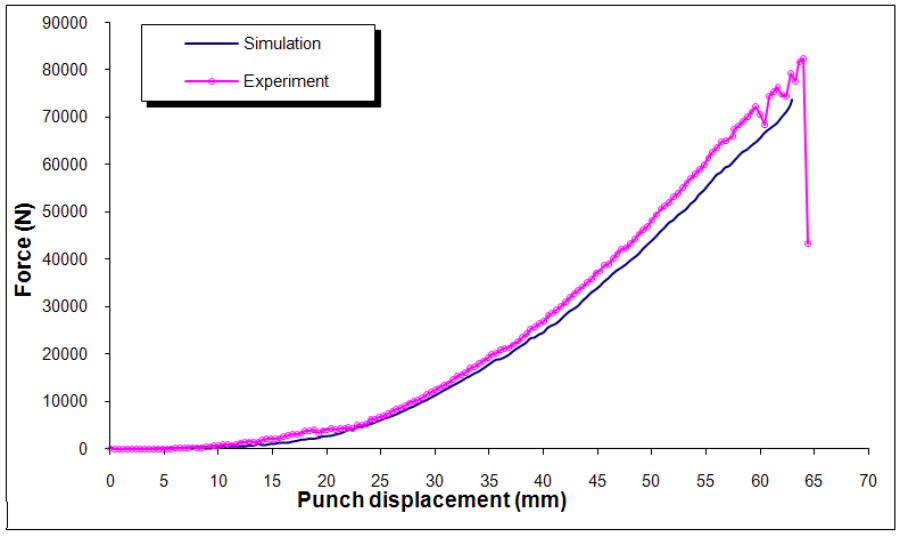


Figure 22. Bursting force versus punch displacement.

### *4.4.2. Stamping of Complex Shape*

The second example concerns the simulation of composite glass fabric stamping with complex tools using the mechanical approach and the computational remeshing procedure. The initial shape of the taffetas woven fabric is (700 mm x 350 mm). The high tensile stiffness along the warp respectively weft yarn direction is introduced via truss elements that connect the nodes of the membrane element. The Young‘s modulus in warp and weft directions is 70.00GPa. The local fibre directions are tracked on the part via a 3D-digital image correlation technique that assesses the intersections of a raster pattern that is painted on the pre-consolidated part along the fibres directions. The geometry of the stamping simulation is shown in Figure 23. The first order triangular T3 and quadrilateral Q4 membrane element type was used for the stamping. The binding force was 30N and the punch stroke was 47mm.

The friction coefficient between the glass fabric and the tools is 0.3. The amounts of draw-in and fiber orientation were measured. The fibre direction is assumed (0°/90°). The final deformed shape of (0°/90°) fabric for a 47mm displacement of the punch is shown in figure 24. Numerical simulations obtained with adaptive remeshing are shown in Figures 24a, 24b, 24c and 24d for different remeshing steps corresponding to punch displacement u = 8, 20, 30 and 47mm. We can see that, the initial membrane resin is computed using an initial coarse mesh (5000 Q4 membrane elements), the mesh is again refined uniformly and the adaptive mesh refinement procedure is activated where elements are created automatically in regions of large curvature to even more accurately represent the complex material flow (large stretching) around the punch radii. The final mesh of the resin has 1530 T3 elements and 6131 Q4 elements. The shear angle distribution was plotted in Figure 24e. Figure 24e shows the adapted mesh of the warp and the weft to the curved shape of the punch. As shown in the Figure 25, maximum shear angle was observed at the highly curved area and such positions were almost same for all simulation cases. From the numerical simulation maximum shear angles was 35°.

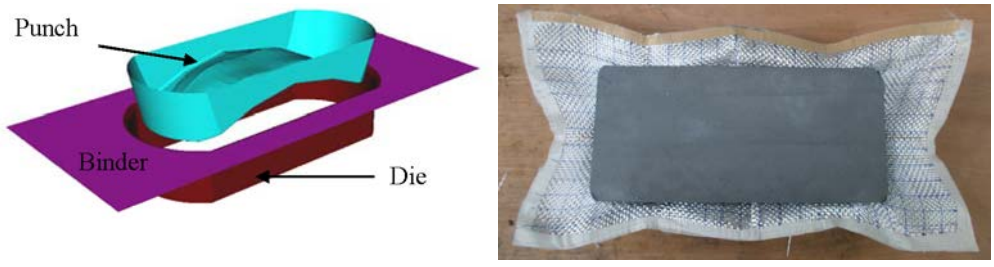


Figure 23. Experimental test of deep-drawing punch shape and final forming.

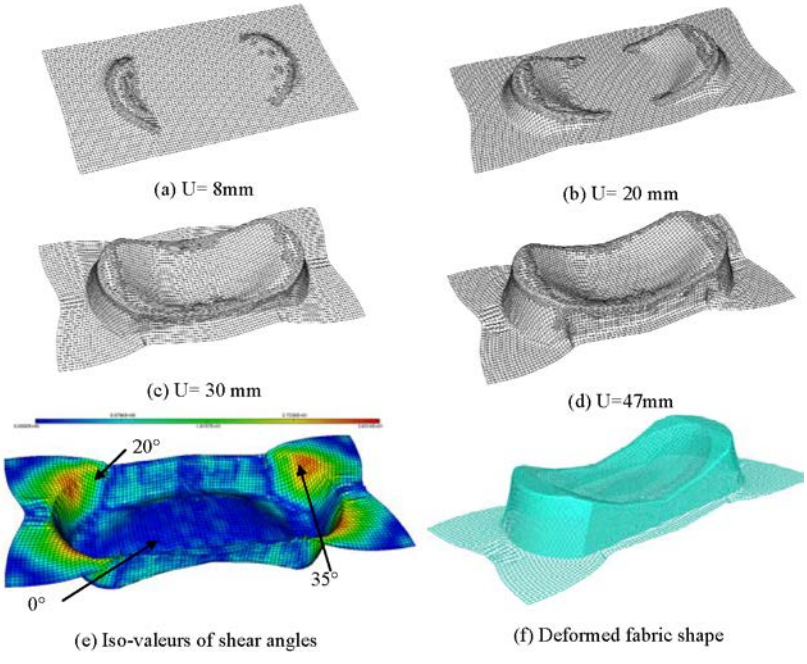


Figure 24. Different mesh of the complex part and shear angles between fibres.

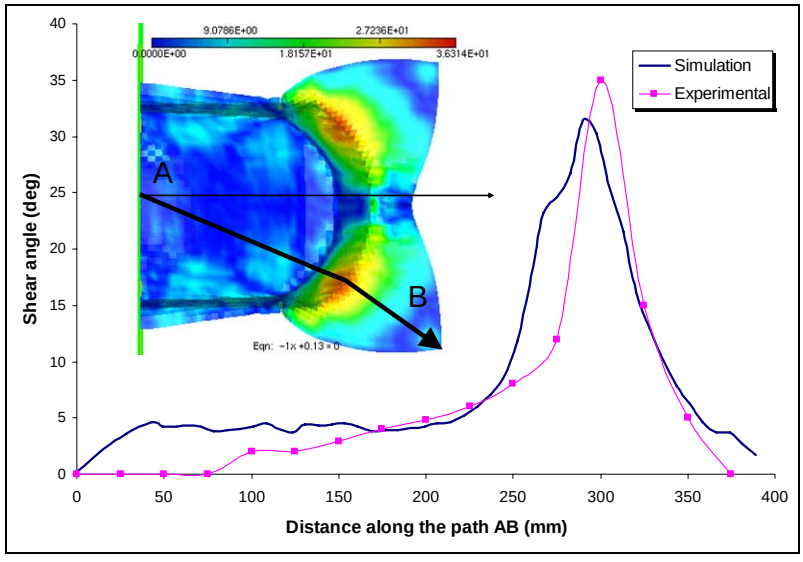


Figure 25. A comparison between experimental and simulated shear angles along the diagonal line.

## CONCLUSION

An important step in the manufacturing processes of thin composite components is the deformation of woven fabric by deep-drawing. The prediction of the angular distorsion of the woven fabric during forming and the changes in fibre orientation are essential for the understanding of the manufacture process and the evaluation of the mechanical properties of the composite structures. An efficient mechanical approach has been presented to simulate accurately the deep-drawing of composite fabric. The mechanical approach is based on a mesostructural model. It allows us to take into account the mechanical properties of fibres and resin and the various dominating mode of deformation of woven fabrics during the forming process (specific deformations of fibre, structural effects of the fabric weaving and the viscosity effects behaviour of the resin). The geometrical approach is based on a modified "MOSAIC" algorithm, which is suitable to generate a regular quad mesh representing the lay-up of the curved surfaces (giving the exact fibre orientations).

The numerical analysis provides input data for the pre-processing of the computation of the final piece after polymerisation and gives the mechanical limits of the fabric during the forming process. Numerical examples concerning the deep-drawing of composite fabric demonstrated the efficiency of the proposed model. An adaptive remeshing technique for composite fabric forming process with refinement and coarsening procedures has been proposed. The implementation with continuum triangular and quadrilateral elements and truss element in the ABAQUS code allows us to validate the proposed approach for several types of problems. Numerical examples concerning the deep-drawing or draping of prepregs composite fabric demonstrated the efficiency of the proposed model.

# REFERENCES


[1] Billoët JL., *Introduction aux matériaux composites à hautes performances*, Teknea, Paris, FR, 1993.

[2] Hou M., Ye L., Mai Y.W. (1997), Manufacturing process and mechanical properties of thermoplastic composite components. *J Mater Process Technol* 63:334–338

[3] Rudd CD and Long AC, *Liguid molding technologies*, Woodhead publishing Limited, 1997

[4] Hsiao SW, Kikuchi N (1999) Numerical analysis and optimal design of composite thermoforming process. *Comp Meth Appl Mech Eng* 177:1–34

[5] George Marsh, *Duelling with composites*, Reinforced Plastics, vol. 50(6), 2006, 18-23.

[6] Trochu, F.; Ruiz E., Achim V., Soukane S. (2006), Advanced numerical simulation of liquid composite molding for process analysis and optimization. *Composites Part A: Applied Science and Manufacturing*, 37, 890-902.

[7] Rajiv Asthana, Ashok Kumar, Narendra B. Dahotre (2006), Composites get in deep with new-generation engine, *Reinforced Plastics*, Volume 50, Issue 11, 26-29.

[8] Boisse P., *Mise en forme des renforts fibreux de composites*, Techniques de l'ingénieur, AM 3734, 2004, 1-10.

[9] Lomov SV, Ivanov DS, Verpoest I, Zako M, Kurashiki T, Nakai H, Hirosawa S (2007) Meso-FE modelling of textile composites: road map, data flow and algorithms. *Compos Sci Technol* 67:1870–1891

[10] Kawabata S., Niwa M., Kawai H., The Finite deformation theory of plain-weave fabrics, *J. Text. Inst*, Parts I, II and III, vol. 64, 1973, p. 21-83.

[11] Lim T.C., Ramakrishna S., Shang H.M., Optimization of the formability of knitted fabric composite sheet by means of combined deep drawing and stretch forming, *J. of Materials Processing Technology*, vol. 89–90, 1999, p. 99-103.

[12] Liu L., Chen J., Li X., Sherwood J., Two-dimensional macro-mechanics shear models of woven fabrics, *Composites Part A*, vol. 36, 2005, p. 105-114.

[13] Rozant O., Bourban P.E., Manson J.A.E., Drapability of dry textile fabrics for stampable thermoplastic performs, *Composites Part A*, vol. 31, 2000, p. 1167–1177.

[14] Hagege B, Boisse P, Billoët JL. Analysis and simulation of the constitutive behavior of fibrous reinforcements. In: *Proceedings of Esaform 7 conference, Trondheim, avril;* 2004. p. 317–20.

[15] Potluri P., Parlak I., Ramgulam R. and Sagar T.V., Analysis of tow deformations in textile preforms subjected to forming forces, *Composites Science and Technology*, vol. 66 (2), 297-305, 2006.

[16] Cherouat A., Gelin J.C., Boisse P., Sabhi H., Numerical modeling of glass woven fabric deep-drawing using finite element method, *Eur J Comput Mech*, vol. 4, 1995, p.159-182.

[17] Cherouat A., Billoët J.L., Mechanical and numerical modelling of composite manufacturing processes deep-drawing and laying-up of thin pre-impregnated woven fabrics, *J. Mat. Proc. Technology*, vol. 118, 460-471, 2001.

[18] Boisse P., Buet K., Gasser A., Launay J., Meso/macro-mechanical behaviour of textile reinforcements for thin composites, *Composites Science and Technology*, vol. 61(3), 2001, 395-401, 2001.

[19] Hamila. N., P. Boisse, Simulations of textile composite reinforcement draping using a new semi-discrete three node finite element, *Composites Part B: Engineering*, vol. 39(6), 999-1010, 2008.

[20] ElHami A., Radi B., Cherouat A., Treatment of the composite fabric's shaping using a Lagrangian formulation, *Mathematical and Computer Modelling*, vol 49(7-8), 2009, 1337-1349, 2009.

[21] Warby M.K., Whiteman J.R., Jiang W.-G., Warwick P., Wright T., *Finite element simulation of thermoforming processes for polymer sheets, Mathematics and computers in simulation* vol. 61, 209-218, 2003.

[22] Teik-Cheng Lim, S. Ramakrishna Modelling of composite sheet forming: a review, *Composites Part A: Applied science and manufacturing*, vool.33, 515-537, 2002.

[23] Pickett AK, Creech G, de Luca P (2005), Simplified and advanced simulation methods for prediction of fabric draping. *Eur J Comput Mech* 14(6–7):677–691

[24] Boisse P, Gasser A, Hagege B, Billoet JL (2005) Analysis of the mechanical behaviour of woven fibrous material using virtual tests at the unit cell level. *Int J Mater Sci* 40:5955–5962

[25] Cherouat A, Borouchaki H, Billoët JL (2005) Geometrical and mechanical draping of composite fabric. *Eur J Comput Mech*, vol. 14 (6–7), 693–708

[26] Mark C, Taylor HM, The fitting of woven cloth to surfaces. *J Text Inst vol*. 47; 477–488, 1956.

[27] Van Der Ween F (1991) Algorithms for draping fabrics on doubly curved surfaces. *Int J Numer Methods Eng*, vol. 31, 1414-1426, 1991

[28] Long AC, Rudd CD, A simulation of reinforcement deformation during the production of preform for liquid moulding processes. *Proc Inst Mech Eng Part B J Eng Manuf vol.* 208, 269-278, 1994

[29] Cherouat A, Borouchaki H, Billoët JL, Geometrical and mechanical draping of composite fabric. *Eur J Comput Mech* 14 (6–7): 693–708, 2005

[30] Borouchaki H., Cherouat A., Drapage géométrique des composites, *C.R. Acad. Sci. Paris, Série II B, mécanique des solides et des structures*, vol. 331, 2003, 437-442.

[31] Harrison P., Clifford M.J., Long A.C., Rudd C.D., A constituent-based predictive approach to modelling the rheology of viscous textile, *Composites Part A*, vol. 35, 2004, 915-931.

[32] S.G. Hancock' ' and K.D. Potter, Inverse drape modelling—an investigation of the set of shapes that can be formed from continuous aligned woven fibre reinforcements , *Composites Part A: Applied Science and Manufacturing* vol. 36(7), 947-953, 2005.

[33] K. Vanclooster, S.V. Lomov, I. Verpoest, Experimental validation of forming simulations of fabric reinforced polymers using an unsymmetrical mould configuration *Composites Part A: Applied Science and Manufacturing*, vol. 40(4), 2009, 530-539

[34] P. Potluri, S. Sharma, R. Ramgulam, Comprehensive drape modelling for moulding 3D textile preforms, *Composites Part A: Applied Science and Manufacturing*, vol. 32(10), 2001, 1415-1424

[35] Spencer AJM (2000) Theory of fabric-reinforced viscous fluid. *Compos Part A* 31:1311–1321

[36] Yu WR, Pourboghrat F, Chung K, Zamploni M, Kang TJ (2002) Non-orthogonal constitutive equation for woven fabric reinforced thermoplastic composites. *Compos Part A* 33:1095–1105

[37] Xue P, Peng X, Cao J (2003) A non-orthogonal constitutive model for characterizing woven composites. *Compos Part A* 34:183–193
[38] Peng X, Cao J (2005) A continuum mechanics-based nonorthogonal constitutive model for woven composite fabrics. *Compos Part A* 36:859–874
[39] Hagège B, Boisse P, Billoët J-L (2005) Finite element analyses of knitted composite reinforcement at large strain. *Eur J Comput Mech* 14(6–7):767–776
[40] Ten Thije RHW, Akkerman R, Huetink J (2007) Large deformation simulation of anisotropic material using an updated Langrangian finite element method. *Comput Methods Appl Mech Eng* 196(33–34):3141–3150
[41] Durville D (2002) Modélisation par éléments finis des propriétés mécaniques de structures textiles: de la fibre au tissu. *Eur J Comput Mech* 11(2–3–4):463–477
[42] Sharma SB, Sutcliffe MPF (2004) A simplified finite element model for draping of woven material. *Compos Part A* 35:637–643
[43] Duhovic M, Bhattacharyya D (2006) Simulating the deformation mechanisms of knitted fabric composites. Compos Part A 37– 11:1897–1915 28 *Int J Mater Form* (2008) 1:21–29
[44] Ben Boubaker B, Haussy B, Ganghoffer JF (2007) Discrete models of woven structures. Macroscopic approach. *Compos Part B* 38:498–505
[45] Borouchaki H., Cherouat A., Billoët J.L., *GeomDrap New Computer Aided Design and Manufacturing for Advanced Textile Composites*, Version 1, 1999.
[46] BenNaceur I., Cherouat A., Borouchaki H., Bachmann J.M, Caractérisation et modélisation de l'aptitude à la déformation des structures souples, *Revue des Composites et des Matériaux Avancés*, vol. 13 (3), 231-240, 2003.
[47] Umer R., Bickerton S. and Fernyhough A., Modelling the application of wood fibre reinforcements within liquid composite moulding processes, Composites Part A: *Applied Science and Manufacturing*, vol. 39 (4), 624-639, 2008.
[48] Vilnis Frishfelds F., Staffan Lundström T. and Jakovics A., Bubble motion through non-crimp fabrics during composites manufacturing, *Composites Part A: Applied Science and Manufacturing*, vol. 39(2), 243-25, 2008.
[49] Long A. C., Process modelling for liquid moulding of braided performs, *Composites Part A: Applied Science and Manufacturing*, vol. 32(7), 941-953, 2001.
[50] Fan J.P., Tang C.Y., Tsui C.P., Chan L.C. and Lee T.C., 3D finite element simulation of deep drawing with damage development, *International Journal of Machine Tools and Manufacture*,vol. 46(9), 1035-1044, 2006.
[51] Jauffrès D., Morris C. D., Sherwood J.A. and Chen J., Simulation of the thermostamping of woven composites: mesoscopic modelling using explicit FEA codes, *Int J Mater Form*, vol. 2(1) 173-176, 2009.
[52] Borouchaki H., Cherouat A., Laug P., Saanouni K. Adaptative meshing for ductile fracture prediction in metal forming, *Comptes Rendus Mecanique*, vol. 330(10), 709-716, 2002.
[53] Giraud-Moreau L., Borouchaki H., Cherouat A., Remaillage adaptatif pour la mise en forme des tôles minces, C.R. Acad. Sci. Paris, Serie II B, *Mécanique des Solides et des Structures*, vol. 333(4), 371-378, 2005.
[54] Cho, J.-W., Yang, D.-Y., A mesh refinement scheme for sheet metal forming analysis, *Proc. of the 5th International Conference*, NUMISHEET'02, 2002, 307-312.

[55] Fourment, L., Chenot J.-L., "Adaptive remeshing and error control for forming processes", *Revue européenne des éléments finis* 3, 2, 1994, 247-279.
[56] Cherouat A. Borouchaki H, Giraud-Moreau L., Mechanical and geometrical approaches applied to composite fabric forming, *Int J Mater Form*, DOI 10.1007/s12289-010-0692-5.
[57] Bergsma O.K., Huisman J., Deep Drawing of fabric reinforced thermoplastic, *2nd Inter. Conf. Comp. Aided Design in Composite Material Technology*, 323-333, 1988.
[58] Benoit Y., Berthé E., Chabin M., Dufort L., Mustapha Ziane M., De Luca P., *Predicting mechanical performance of composite parts though manufacturing simulations*, SAMPE EUROPE 2006.
[59] Abaqus theory, *User's Manual*, 2009.
[60] Gommers B., Verpoest I., Van Houtte P. "Modelling the elastic properties of knitted fabric-reinforced composites", *Composites science and technology*, vol. 56, 685-694, 1996.
[61] Peng X., Cao J., *A dual homogenization and finite element approach for material characterization of textile composites" composites Part: engineering*, vol 33, 45-56, 2002.
[62] Luo Y., Verpoest I. '' Biaxial tension and ultimate deformation of knitted fabric reinforcements" *Composites Part A : applied science and manufacturing* vol 33, 197-203, 2002.
[63] Padmanabhan, K. A. Metal forming at very low strain rates. *Encyclopedia of Materials: Science and Technology*, 2008, pp. 5384-5389.
[64] A. Cherouat and H. Borouchaki, *Present State of the Art of Composite Fabric Forming: Geometrical and Mechanical Approaches, Materials* 2009, vol. 2(4), 1835-1857.
[65] Cherouat, A; Radi, B.; El Hami, A., The Study of the Composites Fabric's Shaping using an Augmented Lagrangian Approach , *Multidiscipline Modeling in Materials and Structures*, vol. 5(2), 185-198, 2009.
[66] R.H.W. ten Thije, R. Akkerman and J. Huétink, Large deformation simulation of anisotropic material using an updated Lagrangian finite element method, *Computer Methods in Applied Mechanics and Engineering*, vol. 196(33-34), 3141-3150, 2007.
[67] Gilormini P., Roudier P., *Abaqus and Finite Strain, Rapport interne n° 140, Cahchan*, France 1993
[68] Dafalias YF, Corotational rates for kinematic hardening at large plastic deformations. *J Appl Mech* 50:561–565, 1983.
[69] Crisfield MA, *Non-linear finite element analysis of solids and structures, II: Advanced topics*. Wiley, New York, 1991
[70] Green AE, Naghdi PM, A general theory of an elastic– plastic continuum. *Arch Ration Mech Anal* 18:251–281, 1965
[71] Dienes JK, On the analysis of rotation and stress rate in deforming bodies. *Acta Mech* 32:217-232, 1997.
[72] Zhu, Y. Y., Zacharia, T., and Cescotto, S., "Application of Fully Automatic Remeshing to Complex Metal Forming Analyses", *Comp. Struct.*, Vol. 62, No. 3, pp. 417-427, 1997.
[73] Gifford, L. N., "More on Distorted Isoparametric Elements", *Int. J. Numer. Meth. Engng.*, Vol. 14, pp. 290-291, 1979.

[74] Babuska, I., Zienkiewicz, O. C., Gago, J. and Olivera D. A., eds., *Accuracy Estimates and Adaptive Refinements in Finite Element Computations*, John Wiley, 1986.

[75] Baker, T. J., "Automatic Mesh Generation for Complex Three-Dimensional Regions Using a Constrained Delaunay Triangulation", *Engineering with Computers*, vol. 5, 1989, pp. 161-175.

[76] Zienkiewicz, O. C. and Zhu, J. Z., "A Simple Error Estimator and Adaptive Procedure for Practical Engineering Analysis", *Int. J. Numer. Meth. Engng.*, Vol. 24, pp. 337-357, 1987.

[77] Oden, J. T., Demkowicz, L., Rachowicz, W. and Westermann, T. A., "Towards a Universal h-p Adaptive Finite Element Strategy, Part 2. A posteriori Error Estimation", *Comp. Meth. App. Mech. Engng.*, vol. 77, pp.113-180, 1989